LUND
UNIVERSITY

Lipid Bilayers on Planes and in Micropipettes -
Two model systems to study binding of DivIVA to flat and negatively curved membranes

60hp MSc Thesis in Physics

Author:
Elisabeth Baumann

Supervisor:
Peter Jönsson

Co-Supervisors:
Jonas Tegenfeldt
Victoria Junghans

Department of Chemistry
Division of Physical Chemistry

Department of Physics
Division of Solid State Physics

Lund University, May 2016
Spring Semester 2016

Abstract

The aim of this thesis work was to form and characterize model systems of cell membranes on planar supports and in micropipettes. Firstly, supported lipid bilayers (SLBs) were formed on glass slides after an existing experimental procedure. It was shown possible to obtain fluid SLBs from different kinds of lipids as well as on glass slides that were cleaned with different techniques. Custom-written MATLAB scripts were used to assess the mobilities of the lipids. It was found that all SLBs showed diffusivities within the same order of magnitude independent of the lipid used, while the fraction of lipids that were immobile within the SLB were higher for *Escherichia coli (E. coli)* compared to POPC lipids. Secondly, a new protocol was established for the lipid-coating of pipettes, which was successfully demonstrated as well. Using again a custom-written MATLAB program to analyze the mobility of the lipids, it was found that they diffused significantly slower than on the planar SLBs. It is suggested that this was due to deficient cleaning or that it could be inherent to the geometry of the lipid bilayer. Additionally, both model systems were used to investigate the membrane binding behavior of the protein DivIVA which is known to localize to regions of high negative curvature in the cell. The results indicated that besides curvature, lipid charge and composition are also features that affect the membrane binding behavior of the protein. Overall, this work presents the groundwork for a cheap model system of the curved cell membrane, which also allows to investigate many different curvature radii at the same time.

Für Opa.

Popular Science Abstract

Whether bacteria or blue whale- every living organism is made up of the common, fascinating building block of life: the cell. It is, as its origin from the Latin word *cella* suggests, a "small room" crammed with all kinds of things. There are for example the cell nucleus containing the DNA with the genetic instructions, the mitochondria as power plants of the cell or the endoplasmic reticulum as an intracellular highway to quickly transport molecules from one place to another. Naturally, the cell is also surrounded by a kind of wall which separates it from its surroundings. This wall, called the cell membrane, was the subject of this thesis work. In principle, it is just a greasy coating, since the membrane is built up of fat molecules - lipids. The lipid is an amphiphilic (Greek *amphis* = both and *philia* = love) molecule which means that one end of it wants to be in contact with water (the head) while another does not (the tail region). Due to this, lipids in water spontaneously assemble into structures in which the lipid heads are exposed to water molecules, while the lipid tails are not. We have all seen this when trying to mix water and fat, like for example in a soup. One of these structures is the lipid bilayer. As the name suggests, it is composed of two chains of lipids facing each other. The cell membrane is therefore simply a lipid bilayer. Simply? Far wrong! While its main component are the lipids, it is also embedding countless different kinds of proteins. These we do not only need to grow muscles, but they also fulfill complex and intertwined functions regarding e.g. intercellular communication or molecule transport into and out of the cell among many others. We were particularly interested in one of the proteins binding to the cell membrane which is called DivIVA. It is found in bacteria that have a rigid cell wall which shapes the fluid cell membrane. DivIVA seems to be involved in regulatory processes for cell division and growth. An interesting feature of it is that it tends to bind to the regions of the membrane that are more curved than others, for example the two ends in a rod-shaped bacterium. Understanding why this is the case will certainly shed light on how the bacterial cell manages to divide exactly in the middle or avoids excessive growth. However, it turns out that it is rather difficult to study DivIVA or other proteins within the living cell, not only because of all the efforts associated with culturing cells but also because of all the intertwined interactions of proteins on the membrane which make it very hard to isolate a particular facet. Therefore, researchers have been utilizing model systems of the cell membrane. The advantage of these is that the conditions, such as the kinds of lipids the membrane is composed of or the concentrations of the proteins present in the systems, are highly controllable and therefore particular issues can be investigated. One of these model systems is the supported lipid bilayer (SLB), which is a lipid bilayer formed on a solid support. The goal of this thesis work was to obtain an SLB from different lipids on a plane glass slide, characterize it regarding its quality (i.e. investigate the movement of the lipids within the SLB) and use it to study the membrane binding behavior of DivIVA. Moreover, it was tried to obtain and char-

acterize a model system of the curved membrane, since DivIVA is known to bind to these. For this, the walls of a glass pipette were coated with a lipid bilayer. Due to the conical shape of the pipette, many different curvatures, higher ones close to the pipette opening and lower ones further away from it, could be utilized to investigate the curved membrane binding preference of proteins such as DivIVA. In this work, I showed it possible to obtain SLBs on glass slides as well as in micropipettes. I investigated DivIVA binding in both systems and found that the charge and type of lipid in the bilayer are important factors affecting DivIVA binding. To put this into a broader context, I showed that lipid-coated pipettes can be used as a model system of the curved membrane. This could be useful to conduct studies under highly controlled experimental conditions not only with DivIVA but also other proteins that are known to preferably bind to curved membranes. An example is the protein α-synuclein which is associated with aggregation in the brain in patients with Parkinson's disease.

List of Abbreviations

B. subtilis	*Bacillus subtilis*
E. coli	*Escherichia coli*
S. coelicolor	*Streptomyces coelicolor*
BLM	black lipid membrane
CA	Cardiolipin
Ct	C-terminus
DHPE	1,2-dihexadecanoyl-sn-glycero-3-phosphoethanolamine
DIC	Differential Interference Contrast
DPPE	1,2-dipalmitoyl-sn-glycero-3-phosphoethanolamine
EDTA	Ethylenediaminetetraacetic Acid
FRAP	Fluorescence Recovery After Photobleaching
GUV	giant unilamellar vesicle
MTS	motorized translation stage
ND	neutral density
Nt	N-terminus
OG®-DHPE	Oregon Green® 488 DHPE
PDMS	Polydimethylsiloxane
PE	L-α-phosphatidylethanolamine
PG	L-α-phosphatidylglycerol
POPC	1-palmitoyl-2-oleoyl-sn-glycero-3-phosphocholine
POPS	1-palmitoyl-2-oleoyl-sn-glycero-3-phospho-L-serine
sCMOS	scientific Complementary Metal-Oxide-Semiconductor
SECM	Scanning Eletrochemical Microscopy

SLB	supported lipid bilayer
SUVs	small unilamellar vesicles
TIRF	Total Internal Reflection Fluorescence
TIRFM	Total Internal Reflection Fluorescence Microscopy
TRIS	Tris(hydroxymethyl)aminomethane
wt%	weight percent

Contents

1 Introduction **1**

2 Theoretical and Experimental Background **5**
2.1 Supported lipid bilayers (SLBs) 5
2.2 Fluorescence microscopy 7
2.2.1 Total Internal Reflection Fluorescence Microscopy (TIRFM) 7
2.2.2 Fluorescence Recovery After Photobleaching (FRAP) 8
2.3 DivIVA 12

3 Methods **15**
3.1 Materials 15
3.2 Microscopy setup 17
3.3 Preparation of SLBs 18
3.3.1 Cleaning glass slides 18
3.3.2 Preparing lipid vesicles 18
3.3.3 Preparing the SLBs 19
3.4 Preparation of lipid-coated micropipettes 19
3.4.1 Pulling and bending pipettes 19
3.4.2 Cleaning pipettes 20
3.4.3 Lipid-coating of pipettes 21
3.5 Conducting a FRAP experiment 22
3.6 Applying pressure to lipid-coated pipettes 23

4 Results and Discussion **25**
4.1 Lipid diffusion in planar supported lipid bilayers 25
4.1.1 SLB formation 25
4.1.2 FRAP experiments on planar SLBs 27
4.2 Lipid bilayers in pipettes 32
4.2.1 Fluorescence imaging of a lipid-coated pipette 32
4.2.2 FRAP experiments in a lipid-coated pipette 35
4.3 Membrane binding of DivIVA 37
4.3.1 DivIVA binding to planar membranes 37
4.3.2 DivIVA binding to negatively curved membranes 40

5 Conclusions and Outlook **43**

Appendices **53**

A Derivation of 1D intensity recovery equation **55**

B Derivation of 2D intensity recovery equation **57**

C MATLAB script: 1D FRAP analysis on planar SLBs **59**

D MATLAB script: 2D FRAP analysis on planar SLBs **65**

E MATLAB script: 1D FRAP analysis on pipette SLBs **71**

Chapter 1

Introduction

The self-assembled lipid bilayer is one of the most remarkable structures found in nature. In form of the cell membrane, a lipid bilayer does not only separate cells from their surroundings but also contains countless types of proteins which regulate, among other functions, the intercellular communication as well as the molecule transport in and out of the cell. Naturally, a research interest has developed to better understand these processes. Since the cell membrane is a complex system hosting many intertwined mechanisms, it is hard to investigate a specific facet *in vivo*, i.e. on the living cell. Therefore, model systems of lipid membranes have been utilized for many experiments. They provide the possibility to study processes and coherences in the cell membrane *in vitro* under highly controllable and tunable conditions with a variety of experimental techniques. One of the main characteristics of the membrane that needs to be conserved in the model systems is the fluidity of the lipid bilayer. According to the fluid mosaic model, the constituents of the membrane, namely lipids and proteins, can laterally diffuse within it [1].

The first utilized model system of a cell membrane was the black lipid membrane (BLM) as introduced by Mueller et al. in the 1960s [2]. The BLM is a lipid bilayer spanning a hole in a hydrophobic support. This is achieved by carefully lowering and then raising a lipid solution over the hole, a process called painting. The name "black" lipid membrane refers to the dark appearance of the BLM in optical microscopy. Light reflected from the front interferes destructively with light reflected from the back due to the small thickness of the lipid bilayer.

In the mid-1980s, the first supported lipid bilayer (SLB) was developed [3]. In contrast to the BLM, the SLB is formed on a solid substrate. Different materials have been investigated regarding their quality as substrates. While hydrophilicity is a necessary condition for SLB formation, it does not seem to be a sufficient one. SLBs form very efficiently on silica, glass and mica but not on e.g. TiO_2 or $SrTiO_2$ even though these materials are hydrophilic as well [4, 5]. Furthermore, several ways to fabricate SLBs have been established. The most common ones are the Langmuir-Blodgett and the vesicle-adsorption technique [4]. In the Langmuir-Blodgett method, the hydrophilic substrate is pulled through a lipid monolayer. To form a lipid bilayer, it is then horizontally pushed onto a second monolayer. In contrast, small unilamellar vesicles (SUVs) adsorb to and rupture on the substrate to form an SLB in the vesicle-adsorption technique.

While in both the BLM and the SLB model system the fluidity of the lipids and embedded proteins is preserved, the SLB is more stable and can be exploited by more experimental techniques [4]. It has since evolved to be a widely used tool to investigate the function and mobility of proteins [5, 6], e.g. during immune cell responses [7].

Over the last couple of years, an interest has emerged to examine membranes and membrane proteins in terms of membrane curvature [8]. By convention, positive curvature is defined as the bending in a lipid monolayer from the polar heads to the tails (e.g. the outside of a lipid vesicle which is exposed to the solvent) and negative curvature as the opposite (e.g. the inside of a lipid vesicle) [9]. It was shown that certain proteins can induce curvature by partially inserting into or imprinting their intrinsic shape onto the membrane, a process called scaffolding [10, 11]. Other proteins can sense membrane curvature, like e.g. the protein α-synuclein associated with Parkinson's disease. It seems to bind to the hydrophobic residues that are especially exposed in positively curved membranes [12].

The protein DivIVA on the other hand, which is conserved across many species of Gram-positive bacteria, is known for localizing to regions of negative curvature in the cell membrane [13]. It has been shown to fulfill several functions concerning cell division and growth [14]. Almost 20 years ago it was found that DivIVA binds to the cell septum and the cell poles in order to ensure proper cell division [15, 16]. More than ten years later, this was associated with the negative membrane curvature at these positions [13,17]. However, so far the membrane binding preference of DivIVA has only been investigated *in vivo* and with simulations [13]. All of this experimental work is time-consuming and the conditions cannot be tuned easily due to the nature of cell culture. Having a model system of a curved cell membrane to study the protein *in vitro* can complement the techniques already exploited.

There already exist numerous model systems of curved membranes. Different groups have exploited a system of a cylindrical lipid bilayer pulled from a giant unilamellar vesicle (GUV) to study membrane curvature effects [18–20]. While these are not based on the concept of SLBs, other systems have been developed that do. Several groups have used Polydimethylsiloxane (PDMS) as a substrate material, which is known to be a cheap option to easily accomplish almost any surface design that can be printed on a wafer. Therefore, they fabricated PDMS devices with groove or even sinusoidal wavy structures on their surface which resembled positively and negatively curved membranes [21–23]. Dabkowska et al. have formed lipid bilayers with high local curvature on vertical nanowires by first growing a nanowire "forest" and subsequently using the vesicle-adsorption technique to form SLBs on them [24]. While it has hence been shown possible to produce and utilize model systems of curved membranes, none of these can be used to study an infinite number of curvature radii at the same time. This would be beneficial, however, when investigating how high the curvature must be for the protein to sense it. To circumvent this problem, the tip of a glass pipette was to be established as a substrate for an SLB in this work, since its conical shape provides a continuous distribution of both negative (inside of pipette) and positive (outside of pipette) curvatures.

Ever since a micropipette was used as microelectrode by Barber in 1902 [25], they have been an established tool used for all kinds of experiments in the life and surface sciences: the controlled localized delivery of molecules to surfaces and even live cells [26,27], sensing and trapping of DNA and other biomolecules [28–30] or to image surfaces with Scanning Eletrochemical Microscopy (SECM) [31] to only mention a few examples. Hernández-Ainsa et al. showed that lipid-coating of pipettes is possible by exposing the capillary tip to a solution containing SUVs such that an SLB could form on the walls by vesicles-adsorption [32]. Afterwards, the bilayer formation was confirmed by means of fluorescence microscopy and current-voltage-characteristics. The system was then used to study the

translocation of DNA and it was found that the performance is improved compared to uncoated capillaries. However, this setup has so far not been used as a model for curved membranes.

One goal of this thesis was to establish a model membrane system that could be used to study the membrane binding behavior of DivIVA *in vitro*. As planar SLBs are not sufficient to investigate all binding properties already recognized *in vivo*, the concept of the lipid-coated micropipette as described above [32] was investigated for this purpose. Using lipid-coated glass pipettes could provide a cheap and easily accessible alternative to study both positive as well as negative curvature preference of proteins in general and DivIVA in particular. Moreover, it makes it possible to investigate - in contrast to most, if not all, other methods presented so far to our knowledge - different curvature radii at the same time.

In order to be able to properly investigate the DivIVA binding behavior, it was essential to obtain high-quality lipid bilayers on plane surfaces as well as in micropipettes. Another main aim of this work was therefore to develop a biophysical toolbox to characterize and study SLBs made on the walls of micropipettes, as well as flat SLBs, by studying the mobility of the lipids in the SLB.

DivIVA binding was also observed on flat SLBs of different composition to better understand how different parameters, such as lipid charge and composition, affect DivIVA binding. Altogether, I show how the combined micropipette-SLB system can be experimentally realized, what to think about when doing this and how this system provides a promising model system of a curved cell membrane. This system could help to further understand, if and why membrane curvature affects the binding behavior of DivIVA, and other proteins, by allowing for *in vitro* experiments to be performed under highly controlled conditions.

Chapter 2

Theoretical and Experimental Background

2.1 Supported lipid bilayers (SLBs)

Every cell is surrounded by a membrane which does not only restrict the size of the cell but also acts as a barrier for ions, proteins and other molecules to leave or enter the cell interior. According to the fluid mosaic model as proposed by Singer and Nicolson, all molecules embedded in the membrane are mobile, i.e. they can freely diffuse [1].

The building blocks of these membranes are phospholipids which are amphiphilic molecules. This means that one part of them is hydrophilic (the head group) while another is hydrophobic (the tail region) as schematically represented in part (a) of Figure 2.1.

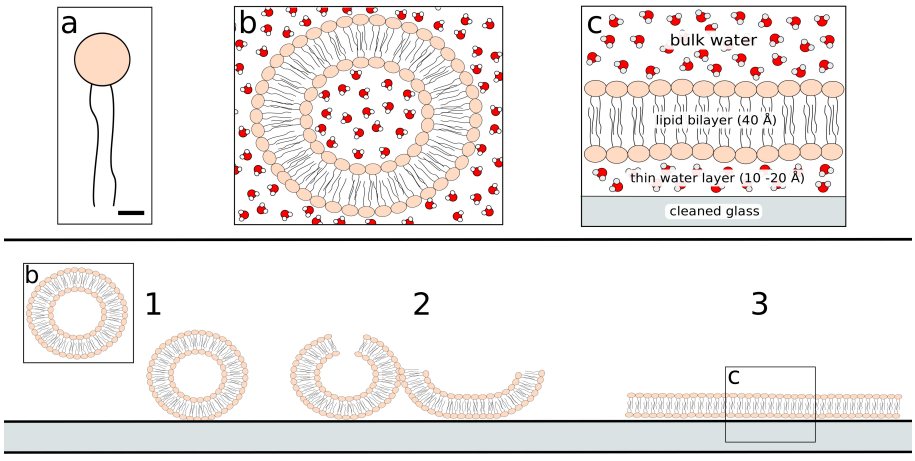

Figure 2.1: *Top:* **a**: A zoom-in of a single building block of any bilayer - a schematic lipid molecule with its hydrophilic head and two hydrophobic tails. The scale bar in the bottom right corner represents several Ångström (an exact length will depend on the kind of lipid, e.g. $\approx$ 1.5 Å for POPC). **b**: A cross-section of a schematic lipid vesicle. The head groups of each lipid face towards the solvent (either the bulk solvent or the one contained by the vesicle). **c**: A zoom-in on the schematic SLB. The thin water film that forms between the bilayer and the solid support ensures the full mobility of all lipids as well as small proteins embedded in the membrane. *Bottom:* Schematic representation of the formation of an SLB by vesicle-adsorption. **1**: Lipid vesicles in solution diffuse toward a cleaned plane glass surface. **2**: The vesicles start to touch each other after enough have landed on the surface. This contact induces a stress which leads to the rupture of the vesicles. **3**: A continuous and fluid bilayer spanning the entire surface forms once enough vesicles have ruptured.

Due to this, phospholipids in solution assemble to form energetically favorable structures for which the head groups are exposed to the solvent, while the hydrophobic tails are not. For the cell membrane, for example, two chains of lipids (each called a monolayer) form a closed bilayer such that the tail regions face each other. A smaller version of a lipid bilayer enclosing solvent is called a lipid vesicle (see part (b) in Figure 2.1).

A supported lipid bilayer (SLB) is a widely used model system resembling the cell membrane [3, 4, 33, 34]. The main advantages of SLBs compared to working with cells *in vivo* are their long lifetime and the high control over the experimental conditions such as lipid composition and concentration as well as membrane proteins present in the system. There exist several ways to fabricate an SLB; the one used for this thesis work is schematically illustrated in the bottom of Figure 2.1. Lipid vesicles in solution are let to diffuse onto a cleaned glass slide. Once they bind to the surface and the coverage is high enough for the vesicles to interact with each other, a stress is induced which causes them to rupture and spread until a uniform bilayer is spanning the entire area [34]. Since the bottom monolayer is not directly touching the glass (but instead a thin water layer separates the two, see part (c) in Figure 2.1), the mobility of the lipids as well as smaller transmembrane proteins is ensured [3, 35].

Besides preparing SLBs on planar supports, I also attempted to coat the walls of a glass micropipette with a lipid bilayer (inspired by Hernandez-Ainsa et al. [36]). This system provides a way to study postively and negatively curved bilayers on the outer and inner pipette wall, respectively. Moreover, the cross-sectional radius R of the pipette increases with distance from the tip, i.e. infinitely many membrane curvatures $c = 1/R$ can be observed at the same time.

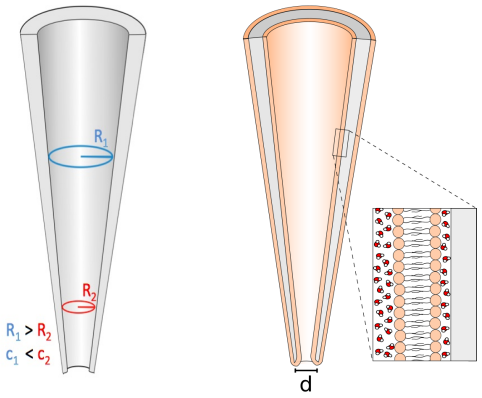

Figure 2.2: Visualization of the different negative curvatures in a conical pipette (the curvature farther away from the tip $c_1 = 1/R_1$ is smaller than the one closer to it $c_2 = 1/R_2$) (*left*) and lipid coating of its walls (*right*). d denotes the diameter of the pipette and was in the µm-range for this work.

This system is of interest because it allows to study the membrane binding behavior of proteins that are curvature sensitive. One of these is DivIVA which tends to localize in the parts of the cell membrane with highest negative curvature [13]. It was investigated for this thesis work and is presented in more detail in Section 2.3.

2.2 Fluorescence microscopy

Epifluorescence microscopy was used to image bilayers as well as proteins. In order to do this, the lipids or proteins needed to be tagged with fluorescent labels, also called fluorophores. Fluorophores are molecules which can adsorb light of a certain wavelength resulting in an electron getting excited into a higher energy level (as visualized in the Jablonski diagram in Figure 2.3). As the electron falls back into the ground state, a photon is emitted. Due to vibrations and collisions with other molecules, however, this photon has a smaller energy than the initially adsorbed one. Consequently, excitation and emission light can be distinguished from each other. A detailed description of the microscopy setup used for this work is presented in Section 3.2 on page 17.

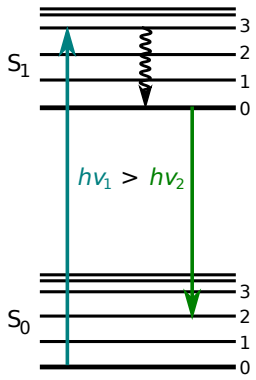

Figure 2.3: *Schematic Jablonski diagram.* The electronic ground state and first excited state are indicated by S_0 and S_1, respectively, while the corresponding vibrational states are represented by the numbers on the right. The electron gets excited from S_0 into S_1 by a photon of energy $E_1 = h\nu_1$. Before it finally relaxes to the ground state under emission of a photon of energy $E_2 = h\nu_2$, the electron first undergoes non-radiating relaxation to the vibrational ground state of S_1 (black wavy arrow). The vibrational states are hence the reason why the emitted photons have a longer wavelength and can be distinguished from the exciting ones.

2.2.1 Total Internal Reflection Fluorescence Microscopy (TIRFM)

The main advantage of an epifluorescence over an ordinary optical microscope is the fact that only the light emitted from the molecules of interest is actually observed. However, fluorescent labeling might alter or even damage the structure of the molecules. Furthermore, when surfaces (like planar SLBs) are to be imaged, fluorescent molecules in the bulk solution are a problem. A way to circumvent at least this drawback is using Total Internal Reflection Fluorescence Microscopy (TIRFM) [37, 38].

It follows from Maxwell's equations that even for total internal reflection a transmitted wave needs to exist [37]. However, as the incident and reflected wave have equal energy, this transmitted wave must not transport away any energy beyond the boundary. The solution is a wave decaying exponentially from the interface, a so-called evanescent wave (a more theoretical treatment of the matter is presented in the review paper by Axelrod et al. [37]). This is the principle exploited by TIRFM (see Figure 2.4). The excitation light is aligned towards the side rather than the middle of the objective in a manner such that it is totally internally reflected at the sample slide. Thus, an evanescent field is created at the sample within a range of a few 100 nm above the surface [38]. The intensity $I(z)$ in dependence of the distance from the slide z can be described as the following exponential

decay [37]:

$$I(z) = I(0) \cdot \exp\left(-\frac{4\pi z}{\lambda_0(n_2^2 \cdot \sin^2(\theta) - n_1^2)^{-1/2}}\right) \tag{2.1}$$

where $I(0)$ denotes the intensity of the incoming light at $z = 0$, λ_0 the wavelength of the excitation light (in vacuum), n_1 and n_2 the refractive indices of the liquid in the sample and the glass, respectively, and θ the incident angle of the incoming light (which needs to be bigger than the critical angle $\theta_c = \sin^{-1}(n_1/n_2)$ for total internal reflection to occur [38]). Therefore, only fluorophores within the field are excited meaning also that only those emitted photons are detectable by the camera.

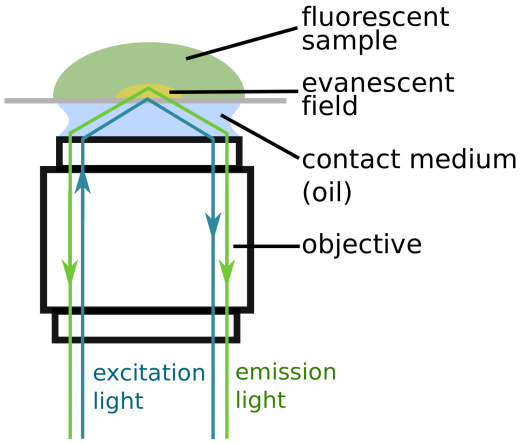

Figure 2.4: *Schematic drawing illustrating the working principle behind TIRFM.* If the excitation light (here blue) is totally reflected at the sample slide, an evanescent wave is created which only excites fluorophores close to the surface. It should be noted that while the excitation light is reflected, the emission photons are radiated in all directions.

2.2.2 Fluorescence Recovery After Photobleaching (FRAP)

A widely used tool to investigate the mobility of fluorescently-labeled molecules is Fluorescence Recovery After Photobleaching (FRAP) as first described by Axelrod et al. in 1976 [39]. In this thesis work, the method was used to quantitatively determine the diffusion coefficients of lipids in planar as well as curved SLBs. Its principle is schematically represented in Figure 2.5. Initially, an SLB consisting at least partially of fluorescently-labeled lipids is prepared (part (a) in Figure 2.5). At time point $t = 0$ (part (b) in Figure 2.5), all fluorophores within a defined area A are photobleached by exposing them shortly to a high-intensity laser pulse at their excitation wavelength. Hence, the overall fluorescence intensity within A will be much smaller than compared to when $t < 0$. Since the lipids are mobile within the bilayer, the photobleached fluorophores start to diffuse out of A while lipids with fluorescently active tags diffuse into it (parts (c) and (d) in Figure 2.6). Therefore, the fluorescent intensity in A recovers to a certain saturation value. A typical recovery curve is shown in Figure 2.6.

In a perfectly fluid bilayer, the recovery will occur to the pre-bleach intensity. Often, however, the recovery is limited by bleached molecules in A that are stuck to the supportive surface and can therefore not diffuse freely. This fraction of immobile molecules is denoted F_{im} in the following, while the fraction of mobile molecules is denoted F_m, respectively.

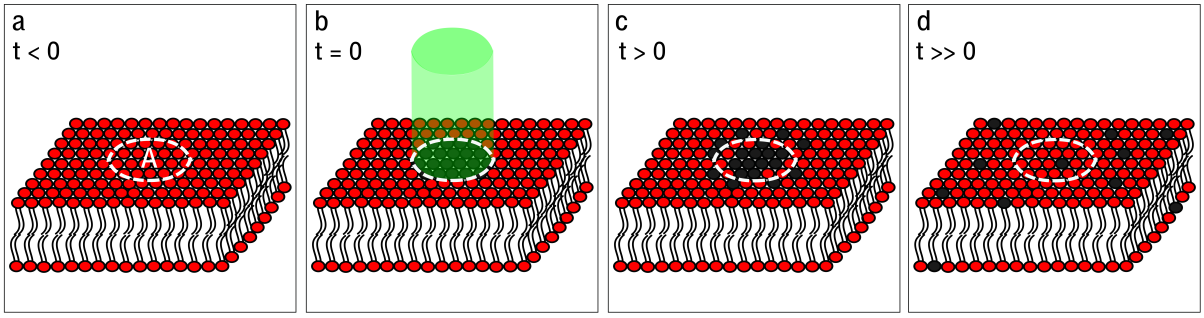

Figure 2.5: *Schematic illustration of a FRAP experiment.* **a**: An SLB consisting of fluorescently labeled lipids (represented by the red head groups) is prepared. **b**: At $t = 0$, a defined area A within the bilayer is exposed to a laser pulse of high intensity. Consequently, all fluorophores in A (on the top as well as on the bottom monolayer) are photobleached (represented by the black head groups). **c**: Due to the mobility of the lipids, bleached fluorophores start to laterally diffuse out of A shortly after the laser pulse while fluorescing ones diffuse into it. **d**: As time progresses, the bleached lipids spread out more and more across the SLB. This results in an overall recovery of the intensity within A.

F_m and F_{im} can be calculated as follows:

$$F_m = \frac{I_E - I_0}{I_I - I_0} \tag{2.2}$$

and

$$F_{im} = 1 - F_m, \tag{2.3}$$

where I_E designates the plateau value (i.e. the recovered intensity as $t \to \infty$), I_0 the intensity at $t = 0$ and hence right after bleaching, and I_I the initial intensity before bleaching (see also Figure 2.6).

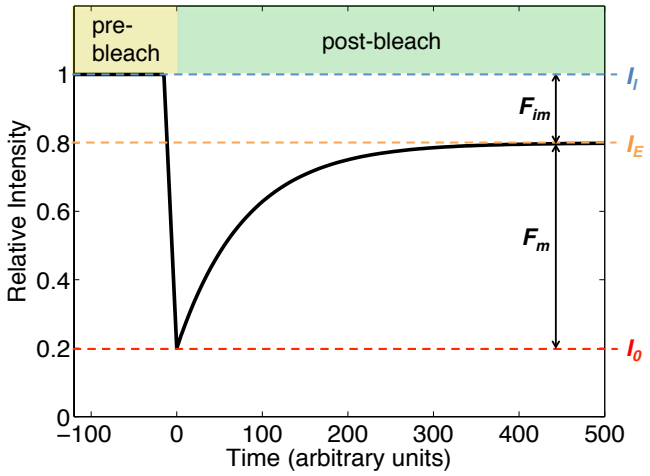

Figure 2.6: *Characteristic intensity curve of a FRAP experiment (solid black line).* The graph shows the distinction between the pre-bleach and post-bleach time ranges before and after the laser pulse, respectively. It furthermore illustrates all quantities appearing in Equations 2.2 and 2.3: the fractions of mobile and immobile molecules (F_m and F_{im}), the initial intensity in the area A prior to bleaching (I_I), the intensity in A right after the exposure to the laser (I_0) as well as the final saturation intensity of the recovery (I_E).

How fast I_E is reached provides information about the diffusion coefficient D of the lipids composing the bilayer [40–42]. In order to understand how D can be extracted from FRAP data, the basics of diffusion theory need to be laid out first.

Generally, D increases with increasing temperature T and decreasing friction:

$$D = \frac{k_B T}{\xi}. \tag{2.4}$$

In Equation 2.4, k_B is Boltzmann's constant and ξ the frictional coefficient which depends on the geometry of the particle of interest and the viscosity η of the surrounding medium. For a spherical particle of radius R, Equation 2.4 becomes the Stokes-Einstein equation [43, 44]:

$$D = \frac{k_B T}{6\pi\eta R}. \tag{2.5}$$

Adolf Fick was the first one to relate diffusion to particle flux and concentration change over time in his famous laws postulated in 1855. In absence of convective motion, Fick's first law states that the particle flux J is equal to the product of D and the negative gradient of the concentration c [45]:

$$J = -D\nabla c. \tag{2.6}$$

Fick's second law describing the concentration change over time is easily derived using Equation 2.6 and reads [45]:

$$\frac{\partial c}{\partial t} = -\nabla J = D\Delta c. \tag{2.7}$$

Returning now to the quantitative FRAP analysis, the fluorescence intensity I within the bleached spot is proportional to the molecular concentration c. It becomes then evident that in order to extract the diffusion coefficient of the lipids, the recovery data needs to be fitted to the solution of Equation 2.7 with the appropriate initial conditions (and assuming an infinite reservoir of fluorescent molecules as boundary condition). For the presented work, two different approaches are taken to extract D. By bleaching either an area in the shape of a rectangle or of a circle, one-dimensional and two-dimensional diffusion can be investigated, respectively (see Figure 2.7). Therefore, also two different approaches to the analysis are necessary.

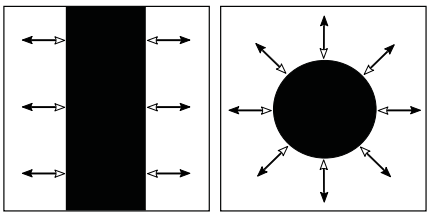

Figure 2.7: *Graphic illustrating the difference between bleaching an area of the shape of a rectangle or a circle. Left:* If the bleached area A has the shape of a rectangle, the intensity within A can only change as lipids attached to photobleached or active fluorophores diffuse along the x-axis. Therefore, one-dimensional diffusion is investigated in this scenario. *Right:* In the case of a bleached circle, however, the intensity recovery is induced by the two-dimensional diffusion of the lipids.

In both scenarios, the initial condition is given by the normalized line intensity profile across the slide right after photobleaching which is fitted to the following Gaussian equation [46]:

$$I_r(r) = I_I \left[1 - K \exp\left(-\frac{(r-b)^2}{w^2}\right)\right]. \tag{2.8}$$

In Equation 2.8, I_I denotes the intensity in the unbleached region, K is a measure for the amount of bleaching, b is the position of the minimum along the x-axis and w is a measure for the width of the bleached area. Note also that for the one-dimensional case $(r-b)^2 = (x-b)^2$, while in two dimensions $(r-b)^2 = (x-b_x)^2 + (y-b_y)^2$ (with b_x and b_y denoting the position of the intensity minimum in x- and y-direction, respectively).

If the bleached area has the shape of a rectangle, the solution of Equation 2.7 evaluated at the center of the bleached region (where $x = b$) can be shown to be (see Appendix A for a derivation) [47]:

$$I_{1D}(t) = I_I \left(1 - K\sqrt{\frac{w^2}{w^2 + 4Dt}} - c\right), \tag{2.9}$$

where K and w were taken as determined in Equation 2.8, I_I represents again the intensity before bleaching and D the diffusion coefficient. The term containing c takes into account the existence of the immobile fraction for which $D = 0$.

For the circle, on the other hand, solving Equation 2.7 using Equation 2.8 as the inital condition yields:

$$I_{2D}(r,t) = I_I \left(1 - K\frac{w^2}{w^2 + 4Dt} \exp\left(-\frac{r^2}{w^2 + 4Dt}\right)\right). \tag{2.10}$$

Integrating Equation 2.10 from 0 to R and incorporating a term for the immobile fraction with factor c then yields for the intensity recovery in a bleached circle of radius R [46, 48]:

$$I_{2D}(t) = I_I \left(1 - K\frac{w^2}{R^2}\left[1 - \exp\left(-\frac{R^2}{w^2 + 4Dt}\right)\right] - c\frac{w^2}{R^2}\left[1 - \exp\left(-\frac{R^2}{w^2}\right)\right]\right). \tag{2.11}$$

A derivation of Equations 2.10 and 2.11 is presented in Appendix B.

Moreover, the formula for F_{im} simplifies to the following expression by using that $I_E = I_{iD}(t \to \infty)$ and $I_0 = I_{iD}(t = 0)$ (for $i = 1, 2$):

$$F_{im1D/2D} = 1 - F_m = 1 - \frac{K}{K + c} = \frac{c}{K + c}. \tag{2.12}$$

2.3 DivIVA

DivIVA is a protein which is highly conserved in Gram-positive bacteria, i.e. bacteria that give positive results in a Gram staining test [49] due to their thick cell walls. It is associated with different functions in various species concerning cell division, sporulation and cell growth.

In the rod-shaped bacteria *Bacillus subtilis* (*B. subtilis*), DivIVA was shown to be involved in recruiting chromosomes to the cell poles during sporulation while ensuring that the cell is divided in the middle for cell division [14]. Therefore, *B. subtilis* DivIVA needs to localize at the cell poles and cell division sites which are in fact also the loci with highest negative curvature in the cell membrane [13]. If and how exactly the protein achieves this and whether it senses negative membrane curvature still remains unresolved. Due to its small size (roughly 30 nm when fully extended) compared to the cell, it is likely to form higher-order structures in order to sense any membrane curvature [14]. By determining the crystal structure of *B. subtilis* DivIVA, some interesting structural features have been revealed. It was found that the N-terminus (Nt) contains amino acids responsible for membrane binding [13,50]. The amino acid chain in the Nt forms a coiled-coil dimer [50] (see purple helices wrapped around each other in Figure 2.8). In addition to the α-helix, each monomer also consists of a loop sequence which is rather unstructured. In the dimer, these two loops form a peculiar crossed-over structure (see yellow part in Figure 2.8) which leads to a high exposure of several residues to the solvent. Most striking are two (one in each monomer) hydrophobic phenylalanines (F17). Due to the energetic favorability it has been proposed that these insert into the membrane. Moreover, it seems that electrostatic interactions between the likewise exposed positively charged arginines (R18) as well as lysines (K15) and the negatively charged cell membrane might yield more stable binding [50].

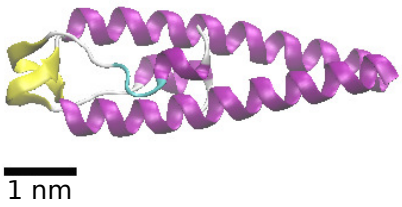

Figure 2.8: *Structural representation of the N-terminus domain of* B. subtilis *DivIVA as determined by Oliva et al.* [50]. Especially interesting for membrane binding is the crossed-loop structure (here colored in yellow). It leads to the exposure of each a hydrophobic phenylanaline (F17) and a positively charged arginine (R18) per monomer to the solvent. F17 is thought to insert into the negatively charged cell membrane while R18 and K15 stabilizes the complex. The image was rendered using the program VMD [51] (from the PDB-file with file-ID 2WUJ).

Another interesting feature has been discovered about *Streptomyces coelicolor* (*S. coelicolor*) DivIVA which was investigated in this work. These filamentous bacteria grow by forming small bulges in the cell wall which start to extend like branches on a tree [52] (see Figure 2.9). How the cell determines where these filaments start to form is not fully understood but it seems that DivIVA plays an important role in the process as it localizes at the tips of the cell as well as the bulges which start to branch [52,53]. These are again the sites of highest negative curvature in the cell membrane.

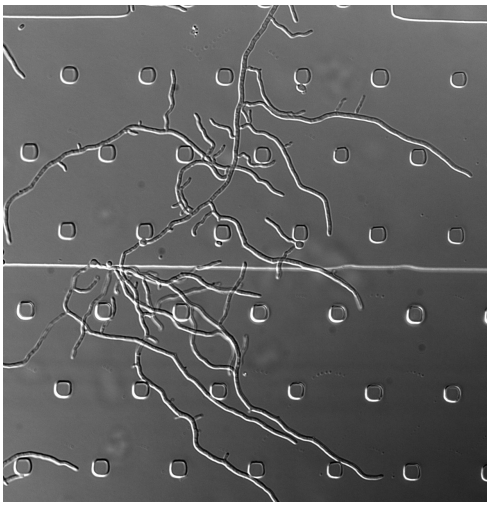

Figure 2.9: *Differential Interference Contrast (DIC) microscopy image of wild type* S. coelicolor. The distance between two adjacent posts is 20 µm. Image courtesy of Dr. Fanny Passot from the Microbiology group at the Department of Biology at Lund University.

Chapter 3

Methods

3.1 Materials

Different types of non-fluorescent lipids were used to generate supported lipid bilayers: (i) 1-palmitoyl-2-oleoyl-sn-glycero-3-phosphocholine (POPC), (ii) 1-palmitoyl-2-oleoyl-sn-glycero-3-phospho-L-serine (POPS), and (iii) *Escherichia coli* (*E. coli*) total lipid extract, which comprised a mixture of lipids that are naturally abundant in the cell membrane of *E. coli* bacteria (57.5% *E. coli* L-α-phosphatidylethanolamine (PE), 15.1% *E. coli* L-α-phosphatidylglycerol (PG), 9.8% *E. coli* Cardiolipin (CA) and 17.6% of unknown lipids). All lipids were obtained from Avanti® Polar Lipids, Inc. Their characteristics which were important for the conducted experiments are summarized in Table 3.1.

Table 3.1: *Summary of lipid characteristics.*

Lipid	Structure	Net Charge
POPC	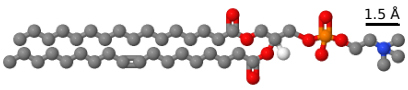	0
POPS	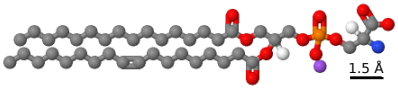	negative
E. coli extract:		
57.5% PE	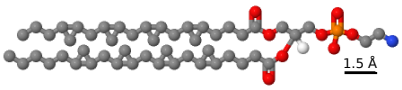	negative
15.1% PG	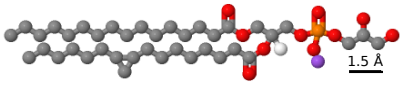	negative
9.8% CA	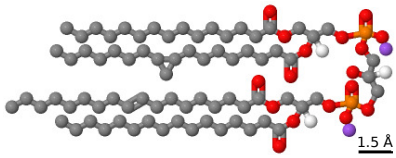	negative

The net charge of the lipids was crucial due to the membrane binding mechanism of DivIVA proposed by Oliva et al. [50] involving positively charged amino acids (see Section 2.3). All structural data was obtained from Avanti® Polar Lipids [54] and visualized using the program Jmol [55].

To get partially fluorescently labeled vesicles, the following lipids, which had a fluorescent dye attached to their head group, were mixed to a concentration of 0.01-0.1 weight percent (wt%) with the other lipid species: (i) Oregon Green® 488 1,2-dihexadecanoyl-sn-glycero-3-phosphoethanolamine (DHPE) which was excited by a 488 nm-laser (see Section 3.2), and (ii) Atto 647N which was excited by a 638 nm-laser. Oregon Green® 488 DHPE (OG®-DHPE) was obtained from Molecular Probes™, and Atto 647N DHPE from Sigma-Aldrich®. The excitation and emission spectra of the two fluorescent dyes are presented in Figure 3.1.

Moreover, the membrane binding behavior of *S. coelicolor* DivIVA was to be investigated. The protein was expressed and purified according to a slightly modified version of the NEB IMPACT™ protocol (New England Biolabs® Inc., Catalog #E6901S) [56].[1] DivIVA was fluorescently labeled with the protein mNeonGreen which could be excited with the 488 nm-laser of the microscope (see Section 3.2). Its absorbance and emission spectra are also presented in Figure 3.1.

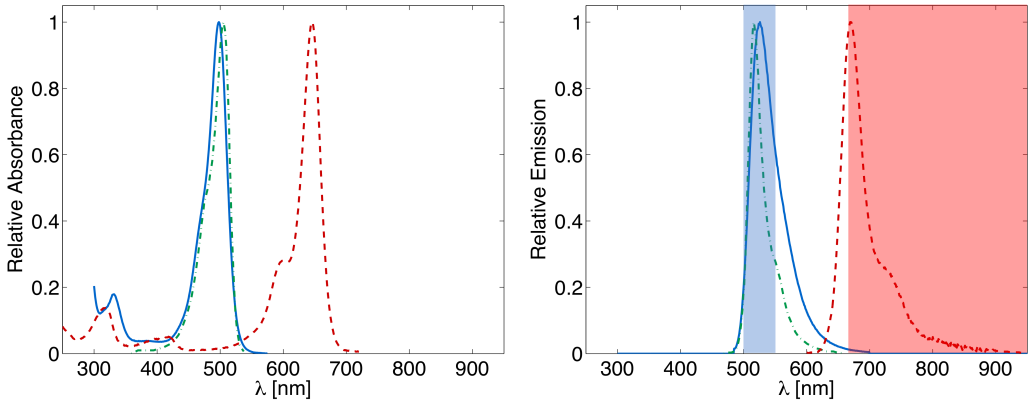

Figure 3.1: *Left:* Excitation spectra for Oregon Green® 488 (solid blue line), mNeonGreen (green dash-dot line) and Atto 647N (dashed red line). *Right:* Emission spectra of the three fluorescent dyes. The colored areas represent the wavelengths let through by the emission filters for the two lasers (blue: 488 nm, red: 638 nm) used in the microscopy setup (see Section 3.2).

Depending on the type of lipid that was used to obtain an SLB, different buffers had to be utilized. For lipid bilayers from POPC or mixtures of POPC and POPS, the buffer had the following composition: 150 mM of NaCl and 10 mM of Tris(hydroxymethyl)aminomethane (TRIS) (pH 8.0). To get SLBs composed of *E. coli* lipids, the buffer did not only contain 150 mM NaCl and 10 mM TRIS but additionally also 20 mM of $CaCl_2$ (pH 8.0). The positively charged calcium ions Ca^{2+} enabled the SLB assembly by forming a sandwich layer between the negatively charged glass surface and the negatively charged lipids which would otherwise repel each other. Furthermore, DivIVA-mNeonGreen was provided in the following buffer: 20 mM TRIS, 150 mM KCl, 1 mM Ethylenediaminetetraacetic Acid (EDTA) and 5 mM $MgCl_2$ (pH 8.0).

[1] This was done by Algirdas Myksis, a Master student supervised by Klas Flärdh in the Microbiology group at the Department of Biology at Lund University.

3.2 Microscopy setup

Epifluorescence microscopy was used to image the fluorescent SLBs and DivIVA. A schematic drawing of the used microscope is shown in Figure 3.2.

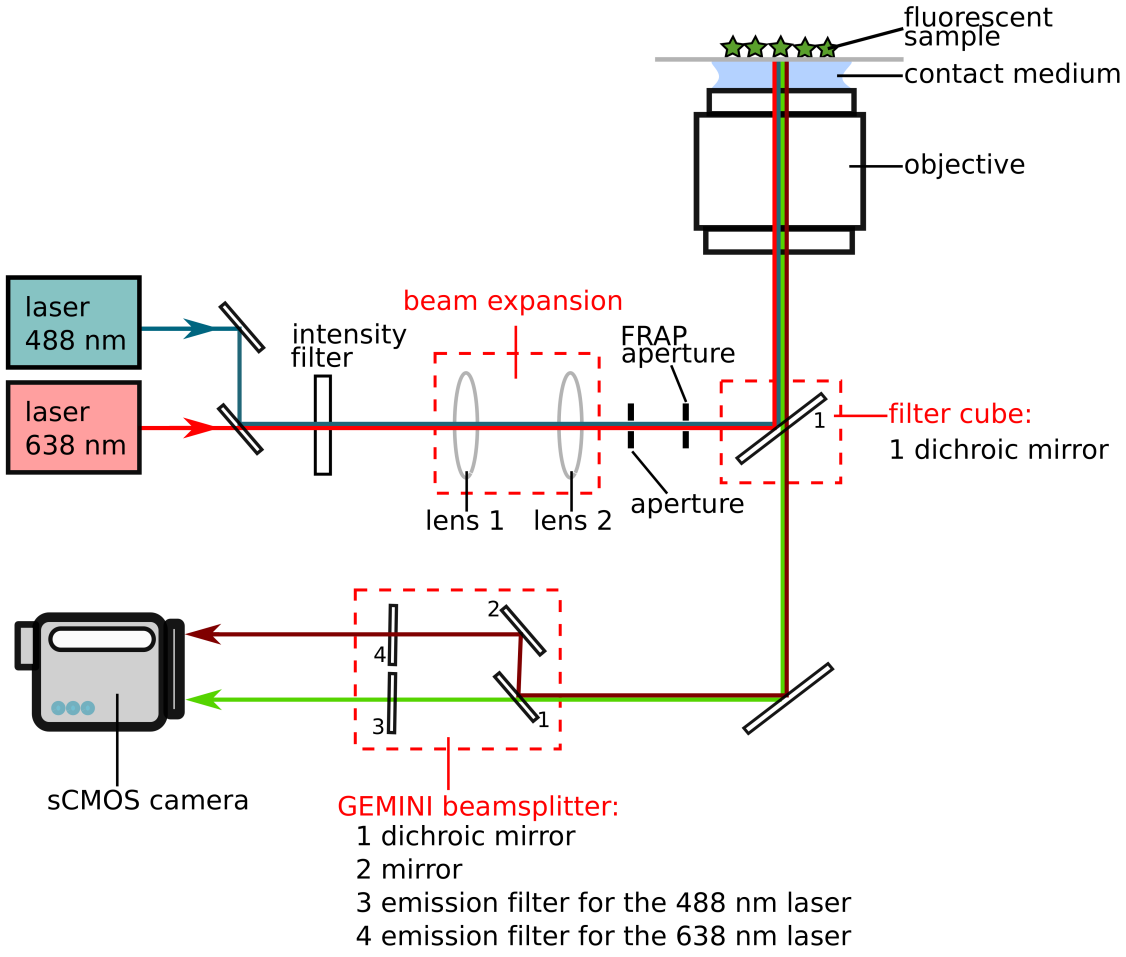

Figure 3.2: *Schematic drawing of the used epifluorescence microscope.* The light of two laser beams is first guided towards a wheel containing different neutral density (ND) filters. Afterwards, the light is expanded by two lenses. The final size of the beams is restricted by an aperture. A second aperture can be placed in the pathway during a FRAP experiment to define the bleached region. A dichroic mirror is used to reflect the excitation light through the objective towards the specimen. In contrast, it is transparent for the emission light which is then guided to the detector, an sCMOS camera. Since the emission light of two different wavelengths is to be observed at the same time, the two beams are separated from each other in a GEMINI beamsplitter. The unlabeled objects in the figure represent optical mirrors reflecting light of all wavelengths. It should also be noted that a periscope and several other beam guiding mirrors (all from Thorlabs) were used in the setup but are omitted in the illustration for reasons of clarity.

Two solid-state lasers (Cobolt AB), one operating at 488 nm and the other operating at 638 nm, generated the excitation light for the fluorescent dyes, Oregon Green® and Atto 647N, respectively. Both lasers were guided along the same pathway before they needed to pass a wheel containing several neutral density (ND) filters (Thorlabs) which could be automatically changed using the program MICROMANAGER. Afterwards, the laser beams were expanded using two lenses (LA1074-A and LA1484 from Thorlabs). A first aperture placed right behind the beam expansion in the pathway was then used to

restrict the beam size to a desired area. A second aperture restricting the beam size even further was affixed to a 90° flip mount (apertures and flip mount provided by Thorlabs). Hence, it could be placed in the pathway when it was needed to define the bleached area in a FRAP experiment (as described in more detail in Section 3.5).

Then, the lasers were guided towards the filter cube in the microscope (microscope model Nikon Eclipse TE2000-U). In contrast to epifluorescence microscopes where no monochromatic light sources are used and an excitation filter is needed to single out the wavelengths absorbed by the fluorophores, the filter cube here consisted only of a dichroic mirror (Di01-R405/488/561/635-25x36 by Semrock). It had several passing bands such that the laser light was reflected towards the objective while the returning fluorescent emission was transmitted. The beam was finally focused onto the sample by the objective (from Nikon, depending on the experiment either an oil immersion or dry objective was used) where the fluorophores within the area of illumination were excited. The emission light was then guided towards a HAMAMATSU DIGITAL sCMOS camera. In order to observe the emission light from two different fluorophores at the same time, it needed to pass through a GEMINI beamsplitter which consisted of a dichroic mirror to separate the rays, a guiding mirror and two emission filters (one for each laser) to suppress any back-scattered excitation or other background light. The microscope as well as the lasers were handled using the program MICROMANAGER.

3.3 Preparation of SLBs

3.3.1 Cleaning glass slides

Glass slides were cleaned using either Piranha solution (a 3:1 mixture of concentrated sulfuric acid H_2SO_4 (95-97 % purity, Merck KGaA) and hydrogen peroxide H_2O_2 (30% purity, Honeywell Burdick & Jackson® Inc.)), ethanol (95% purity, Solveco AB) or acetone (99.9% purity, Honeywell Burdick & Jackson® Inc.).

If Piranha solution was used, the following steps were undertaken: 4.5 ml of H_2SO_4 were added into a glass beaker. Afterwards, 1.5 ml of H_2O_2 were added dropwise into the same beaker. Because mixing of these two chemical compounds is highly exothermic, this step needed to be done very carefully and slowly. Moreover, the solution is only reactive under high temperatures. In order to prevent a lag phase of cleaning, the mixture was therefore preheated for approximately 2 minutes on a heating plate. Finally, the glass slide that was to be cleaned was placed into the solution on the heating plate. After approximately 30 minutes, the glass slide was taken out of the solution, thoroughly rinsed in deionized water and finally dried under gas flow with a nitrogen gun.

If ethanol or acetone were used for cleaning, the glass slide was placed in the respective organic solvent for roughly five minutes. Subsequently, it was also thoroughly rinsed in deionized water and dried under nitrogen flow.

3.3.2 Preparing lipid vesicles

Lipids were usually stored in chloroform at -20 °C (*E. coli* lipid extract at a concentration of 25 mg/ml, all other lipids at 10 mg/ml). For preparing vesicles, 1 mg of lipids was taken from the solution (hence 40 µl for *E. coli* and 100 µl for all other lipids) and filled into a glass vial using a glass syringe. The chloroform was evaporated under nitrogen flow for 30 minutes after which a dry lipid film remained on the bottom of the vial. The

film was rehydrated by adding 1 mL of the desired buffer, such that the final lipid vesicle concentration amounted to 1 mg/ml, and was thoroughly mixed. In order to obtain unilamellar vesicles, the solution needed to be sonicated for 15 minutes. This was done using a sonicator (model VCX 130 from Sonics & Materials, Inc.) at an amplitude of 55% with 10 s pulses, followed by a 10 s waiting time. In order to prevent damage to the sample from heating, it was placed in an ice bath during the entire sonification process.

3.3.3 Preparing the SLBs

In order to fabricate an SLB, 60 µL of the desired buffer was at first added into a silicon well with a diameter of 4.5 mm (Grace Bio-labs, Inc.Press-To-Seal silicon isolators) attached to a cleaned glass slide (a photo is shown in Figure 3.3). The purpose of the silicon well was to allow for small volumes of the needed liquid. Afterwards, 30 µL of lipid vesicle solution (a 1:10 dilution in the desired buffer, final lipid concentration 0.1 mg/ml) were added into the well. By leaving the vesicle solution in the well for approximately 1 hour, it was ensured that a lipid bilayer had formed and the experiments could be conducted (in case of DivIVA membrane binding experiments, the protein was added at this time point). If fluorescently labeled lipids or protein were used, the SLB was imaged using the microscopy setup described in Section 3.2 in TIRF mode employing a Apo TIRF 60x/1.49 oil immersion objective from Nikon.

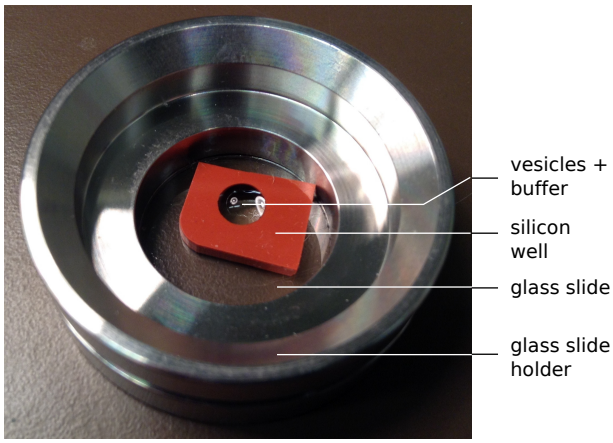

Figure 3.3: *Photo of a silicon well containing lipid vesicles in solution on a cleaned glass slide.*

3.4 Preparation of lipid-coated micropipettes

3.4.1 Pulling and bending pipettes

The pipettes were pulled from Borosilicate Glass Capillaries (World Precision Instruments, outer diameter: 1.0 mm and inner diameter: 0.58 mm) using a Model P-97 Flaming/Brown micropipette puller by Sutter Instruments Co. One glass capillary was placed inside the puller such that its middle was surrounded by a thin heating filament (which is also visualized in Figure 3.4).

As the pulling process was started, the capillary began to melt due to the heating and was tugged stepwise at its ends until it split into two separate pipettes. The heat of the filament, the pulling velocity as well as the time between pulling steps were parameters to be tuned in order to achieve different pipette tip diameters.

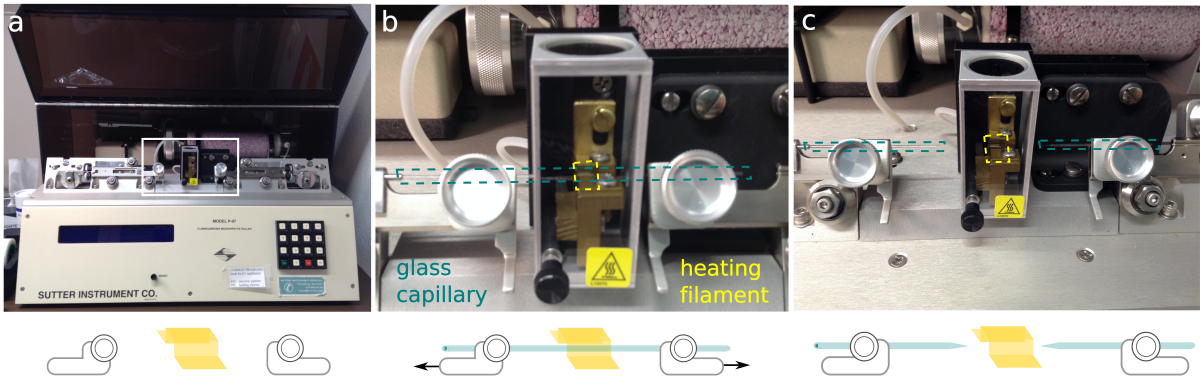

Figure 3.4: *Illustration of the experimental procedure used for pulling pipettes from glass capillaries (photos on the top with simplified graphical representations below).* **a**: The opened pipette puller without a glass capillary. The white box shows the area where the glass capillary is mounted for pulling. On the bottom, the two screws used for tightening the capillary as well as the heating filament (yellow) in the middle are representatively shown. **b**: The glass capillary (framed on the photo by a blue dashed box) is placed inside the puller such that its middle is surrounded by the heating filament. Afterwards, the capillary is alternately heated (which causes melting) and pulled at both ends (indicated by the black arrows in the graphical illustration on the bottom) several times until it breaks apart and two separate pipettes are obtained (**c**). The time span between two heating periods and the pulling velocities can be calibrated in order to achieve different pipette tip diameters.

Because of the setup used for mounting the pipettes onto the microscope (as described below), the pipettes needed to be bent by approximately 90°. In order to do so, the pipette was first horizontally secured with a clamp on a ring stand (see part (a) of Figure 3.5). Subsequently, it was scorched in a confined area (using a Sievert pro-torch) which induced the inclination of the tip part of the pipette (see parts (b) and (c) of Figure 3.5).

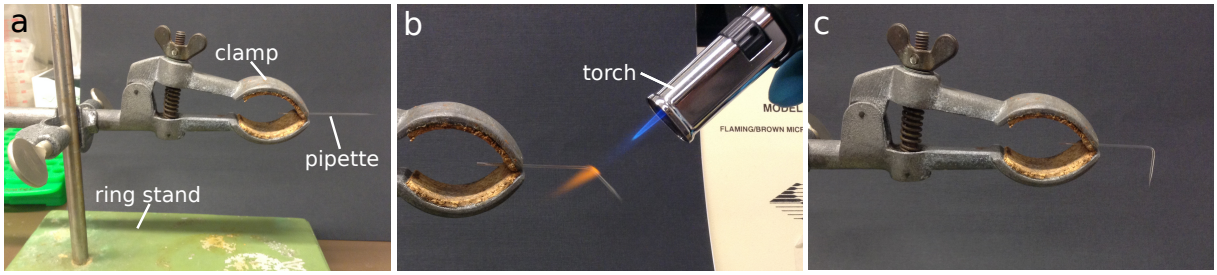

Figure 3.5: *Bending pipettes.* **a**: Before bending, the pipette is fixed to a clamp which is mounted to a ring stand. **b**: By scorching the pipette with a torch, the tip part starts to incline until it is bent by approximately 90° (**c**).

3.4.2 Cleaning pipettes

Similarly to the glass slide used for preparing planar SLBs, the pipettes were cleaned as well for some of the experiment. This was done by placing them (before pulling to avoid breaking the fragile pipette tips) in an ethanol bath for approximately five minutes, thoroughly washing them with deionized water and finally blow-drying them with nitrogen.

3.4.3 Lipid-coating of pipettes

In order to lipid-coat a glass pipette and afterwards image the bilayer, the pipette was first mounted above the microscope on a homebuilt pipette mount. This mount was positioned on a motorized translation stage (MTS25/M-Z8, Thorlabs) with which its vertical position could be controlled. By moving the stage, the pipette was focused in bright-field (using a Plan Fluor 20x/0.50 objective from Nikon). This allowed for easier positioning of the pipette for imaging after a fluorescent bilayer had formed.

Subsequently, the pipette was moved up again and a silicon well attached to a glass slide filled with buffer was placed on the sample holder such that the pipette tip was immersed in the liquid (see part (a) in Figure 3.6). Afterwards, lipid vesicle solution was added to the well.

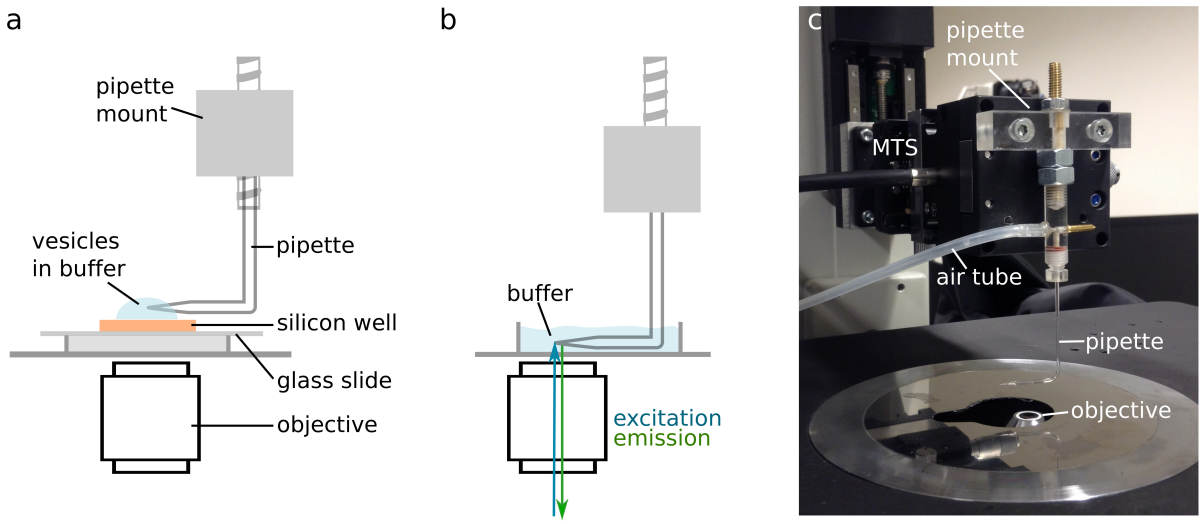

Figure 3.6: **a**: *Setup used to lipid-coat glass pipettes.* The bent pipette is dipped into a lipid vesicle solution contained by a silicon well attached to a glass slide. **b**: *Setup used to image the lipid bilayers in pipettes.* After the pipette tip was immersed in the lipid vesicle solution sufficiently long for a bilayer to form, it was quickly submerged into a buffer reservoir and placed within the range of the focal length of the objective. **c**: *Photo of the setup used to image pipettes.* The air tube was used to apply pressure to the system (see Section 3.6).

To ensure bilayer formation, the setup was left like this for approximately one hour. If binding of DivIVA onto curved membranes was to be investigated, the protein was added into the well at this time point and left to settle for another hour. Afterwards, the silicon well was discarded off and the pipette was moved back to the position at which it was in focus before and simultaneously submerged in an excess buffer reservoir (part (b) in Figure 3.6). However, this step needed to be done quickly to avoid drying out of the bilayer at the outer pipette wall.

3.5 Conducting a FRAP experiment

For performing a FRAP experiment, it was very important to obtain an image before bleaching in order to account for uneven illumination in the subsequent analysis. Afterwards, the second aperture (see Figure 3.2) was placed in the beam pathway by the flip mount. The filter wheel was next switched to an empty state, such that the sample was illuminated by the full laser intensity (60 mW for the 488 nm-laser, 140 mW for the 638 nm-laser) for a short time. Then, the filter was switched back and the aperture was removed from the pathway, and many subsequent images were taken of the whole illuminated area to capture the intensity recovery. The whole process explained above (except operating the flip mount which needed to be done manually) was automated by running a custom-written script in MicroManager.

The quantitative analysis was then performed using different Matlab® scripts (one for the analysis of a 1D FRAP experiment on planar bilayers or in bilayer-coated pipettes, respectively, and one for a 2D FRAP experiment on planar bilayers) developed in this MSc project. All code is provided in Appendices C, D and E of this thesis, respectively. The programs perform roughly the following steps:

1. *Reading in data.* The recovery time series (i.e. the images taken before and after the bleaching) is read into Matlab®.

2. *Obtaining a normalization image.* A dark count of 400 (the intensity value displayed by the camera at zero fluorescence) is subtracted from three images taken before bleaching. Afterwards, these images are averaged to constitute a pre-bleach image.

3. *Fitting of the intensity profile right after bleaching to Equation 2.8.* The image data of the first image taken after bleaching is loaded, the dark count is subtracted and the image is normalized by dividing it by the pre-bleach image. An x-axis intensity profile across the bleached area (averaged over several rows of pixels) is obtained and fitted to Equation 2.8 such that K and w can be extracted.

4. *Extracting the recovery curve from the image data.* The images are loaded successively. The dark count is subtracted from each image. They are also normalized using the pre-bleached image. The intensity either at the center of the bleached region (for 1D analysis) or averaged within the whole bleached area (for 2D analysis) is determined from each image (such that a time series documenting the intensity recovery is obtained).

   One problem that needed to be accounted for was bleaching of the fluorophores over time. Complicating the matter even further, the sample slide was unevenly illuminated (indicated by the different shades of grey from left to right in parts (a1) and (b), respectively, of Figure 3.7) due to slightly imperfect alignment of the laser beam. This implied that the bleaching was more severe on the right side of the sample where illumination was higher than on the left. Since the intensity recovery at the middle of the bleached area was to be investigated for one-dimensional analysis while the integrated intensity was observed for two-dimensional analysis, two different approaches were taken in order to account for bleaching. For the 1D case, the intensity profiles were divided by the intensity values along a line connecting the ends of the profile (see parts (a2) and (a3) of Figure 3.7). In contrast, the intensity inside the bleached region is normalized dividing the intensity in non-bleached regions for 2D analysis (see part (b) of Figure 3.7).

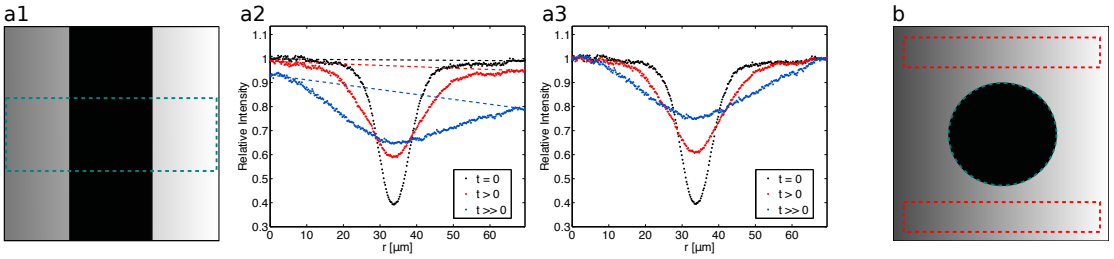

Figure 3.7: *Illustration of how bleaching was accounted for in the FRAP analysis.* **a1-a3**: If the bleached area was a rectangle, the intensities in the middle of the bleached region (i.e. the minimal intensities of the radial profiles along the x-axis) needed to be extracted at every time point. a1 visualizes the bleached rectangle as well as the uneven illumination across the slide. The blue dashed rectangle indicates the area in which the radial intensity is obtained (averaged over several pixel rows). In a2, three representative radial profiles from three different time points are shown. Clearly, bleaching is more severe on the right where illumination is high, especially at later time points (see blue profile). Therefore, the profiles were divided by intensity values along straight lines connecting their ends (dashed lines). a3 shows the same data after accounting for bleaching. **b**: For the 2D case, the intensity inside the bleached region (blue dashed circle) in each image was divided by the average intensity within the red dashed rectangles of the same image. The areas were exposed to the inherent bleaching and since they spanned the whole slide, the affect due to uneven illumination averaged out.

5. *Fitting of the intensity recovery curve to Equation 2.9 or 2.11.* The recovery data is fit to the respective theoretical model. From the fit, the diffusion coefficient D is obtained. Moreover, the fractions of mobile and immobile molecules (F_m and F_{im}) are calculated according to Equation 2.12.

6. *Displaying D, F_m and F_{im} as well as plotting several profiles.*

3.6 Applying pressure to lipid-coated pipettes

Finally, pressure was applied to the lipid-coated pipettes in some experiments. The setup was exactly the same as used for imaging (see Figure 3.6). In principle, the procedure was identical to a FRAP experiment with the exception that right after bleaching the tip, a negative pressure was applied to the pipette (resulting in an inward liquid flow). This was done by connecting a plastic syringe via air tubes to an inlet in the pipette mount (see part (c) in Figure 3.6). By pulling the syringe, pressure was applied to the pipette. Its value was displayed and could hence be controlled by a connected pressure gauge.

If a fluid SLB had formed within the pipette, the shear forces acting on the walls due to the flow caused photobleached lipids to move away from the pipette tip. Hence, another dark spot appeared. To observe the movement of this spot, the intensity line profile along the axis of the pipette $I(x)$ could then be fitted to the following sum of two Gaussians:

$$I(x) = -a \cdot \exp\left(-\frac{(x-b)^2}{d^2}\right) + c - e \cdot \exp\left(-\frac{(x-f)^2}{g^2}\right), \tag{3.1}$$

where $a - g$ were parameters to be fitted.

Chapter 4

Results and Discussion

4.1 Lipid diffusion in planar supported lipid bilayers

4.1.1 SLB formation

Obtaining an SLB (following the protocol presented in Section 3.3 of this thesis) was the groundwork for all experiments that were performed during the course of this MSc thesis.

Since SLBs were a central part of this study, it was started by investigating what an SLB formation looked like. An exemplary image series of a POPC-OG®-DHPE bilayer formation on a Piranha-cleaned glass slide is shown in Figure 4.1. Initially, the vesicles landed on the glass surface and could be seen as small fluorescent dots using TIRFM (see part (a) in Figure 4.1). Once the surface coverage of vesicles was high enough, usually 10-40 minutes after adding the first lipid vesicles to the well, the vesicles started to interact with each other and a nucleation process was started: the vesicles ruptured and formed a SLB that spread across the glass slide (parts (b)-(d) in Figure 4.1).

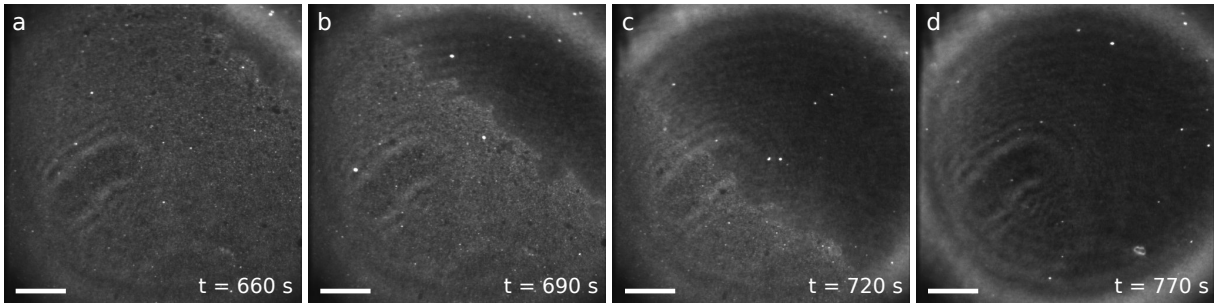

Figure 4.1: *TIRFM images of the SLB formation on a Piranha-cleaned glass slide.* The bilayer starts to spread across the slide from the upper right corner eleven minutes after adding the lipid vesicles into the silicon well. Less than two minutes later it spans the entire illuminated area. It should be noted that the uneven, persistent structure in the left of the images is an artefact arising due to slightly imperfect alignment of the laser and consequent diffraction. The used lipid was POPC (with 0.1 wt% of the fluorescently labeled OG®-DHPE). The scale bars indicate 20 μm.

The SLB formation could also be observed in the change of fluorescence intensity on the slide (see Figure 4.2). At first, the intensity increased as more and more fluorescent lipid vesicles reached the evanescent field and landed on the surface. As they started to rupture, however, the intensity dropped because the number of fluorophores per unit area was now smaller. After the SLB formation, the fluorescent intensity decreased further

due to photobleaching[1] of the fluorophores.

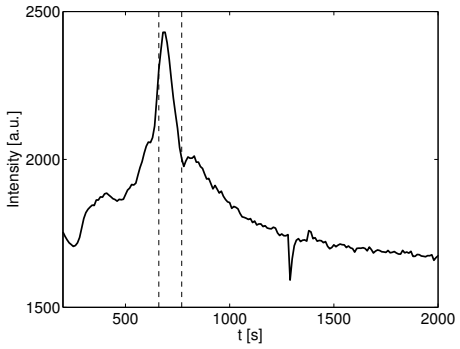

Figure 4.2: *Intensity change over time during the bilayer formation.* At first, the fluorescence intensity within the illuminated area increases because more and more vesicles land on the surface. As nucleation starts (i.e. the vesicles rupture) and the SLB spreads across the slide, the overall intensity decreases (the vertical lines indicate $t = 660$ s and $t = 770$ s, the start and end points of the bilayer formation in Figure 4.1). Afterwards, the intensity decreases further at a different rate due to photobleaching.

Different protocols of cleaning the glass slide have been tested and mobile SLBs were successfully formed with all of them. Generally, the SLB started to form earlier after the lipids were added to the silicon well when the glass slide was cleaned with ethanol or acetone, and later when it was cleaned with Piranha solution. An explanation for this could be that the cleaning procedure using ethanol or acetone, which was much shorter and did not include any heating (see Section 3.3.1 in the Methods chapter), left residues on the glass slide which acted as nucleation sites for the vesicles. Hence, they ruptured more easily when these cleaning agents were used. Another possibility is that Piranha cleaning was more aggressive and resulted in a roughened glass surface such that the area to be covered by the vesicles was higher and consequently the bilayer formation was initiated later.

[1]Photobleaching is a chemical alteration of the fluorophore due to light exposure which leaves it permanently unable to fluoresce.

4.1.2 FRAP experiments on planar SLBs

A large part of the thesis also became to develop analysis methods in MATLAB to be able to obtain diffusion data, i.e. diffusion constant and fraction of immobile molecules, in flat bilayers as well as in pipettes from FRAP experiments. This information was crucial to characterize that an SLB had formed and beyond that served as an indicator for the quality of the SLB. The results were compared between SLBs which (1) were constituted of different kinds of lipids and (2) formed on glass supports that were cleaned using different techniques. Additionally, two different approaches to the quantitative analysis, one contemplating one-dimensional and one contemplating two-dimensional diffusion (as described in Section 2.2.2 and visualized in Figure 2.7), were compared. While the 2D case is the most common way to analyze FRAP data, the 1D case was needed to investigate the diffusivity in the pipette. It was therefore tested on the planar bilayer as well. The results are presented in the following.

One-dimensional diffusion of lipids in planar SLBs

In order to obtain correct values for the diffusion constant and immobile fraction from the analysis on the FRAP images, uneven illumination and fluorescent background signals needed first to be compensated for. This was done by normalizing the FRAP images with the pre-bleach image as described in Section 3.5. Figure 4.3 displays the pre-bleach image (part (a)) as well as an unnormalized (part (b)) and a normalized image (i.e. the result of dividing the unnormalized by the pre-bleach image, part (c)) of the bleached rectangle in a POPC bilayer with 0.01 wt% OG®-DHPE. Additionally, line intensity profiles of the three images are shown. Especially from these it becomes evident that while for the pre-bleach and unnormalized pictures the illumination is clearly uneven across the slide, this effect is eliminated after the normalization. Moreover, the diffraction artefacts are mostly eradicated as well.

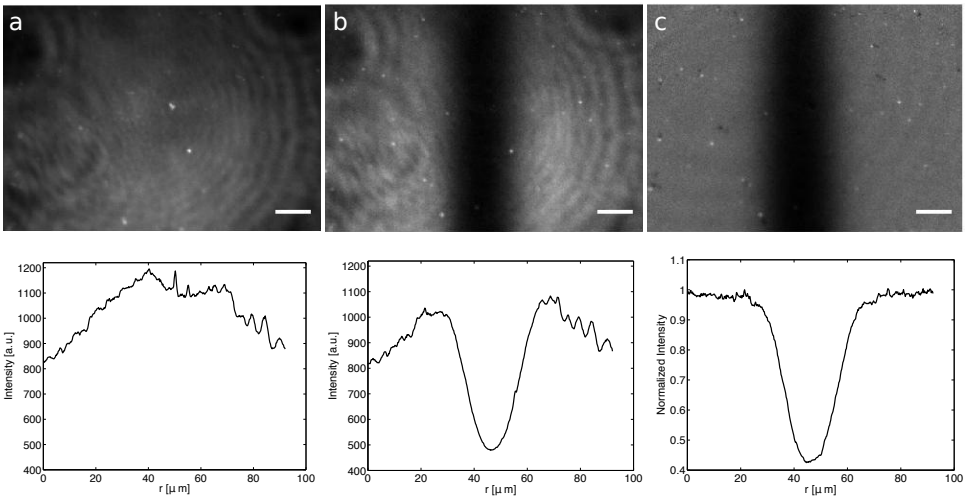

Figure 4.3: *Normalization with the pre-bleach image in a 1D FRAP experiment.* The pictures show the pre-bleach image (**a**) as well as the unnormalized (**b**) and normalized (i.e. the quotient of a and b) image (**c**) of a bleached line with the respective line intensity profile in the bottom. The diffraction artifacts are significantly reduced after normalization resulting in a much smoother image. The scale bars represent 10 µm.

A series of normalized images showing the intensity recovery in a 1D FRAP experiment within the bleached region over time is presented in parts (a)-(c) in Figure 4.4. Whereas

at $t = 0$, right after bleaching, the rectangle has clearly defined edges, they are already blurred after 20 seconds as photobleached lipids diffuse out and non-photobleached lipids diffuse into the bleached region. After 100 seconds, the fluorescence intensity has sufficiently recovered to let the bleached rectangular region disappear. However, the intensity is still lower than at the margins due to molecules that are photobleached but immobile and can therefore not diffuse away.

Finally, the images were analyzed with the goal to obtain D as well as F_{im} using a custom-written MATLAB script, which is presented in Appendix C of this thesis. The program extracted the mimimum of the line intensity profile across the bleached region at each time point (examples of which are presented in part (d) of Figure 4.4) in order to constitute an intensity recovery curve analogously to the theoretical one depicted in Figure 2.6. A fit of the recovery to Equation 2.9 (part (e) of Figure 4.4) output D and was furthermore used to determine F_{im} according to Equation 2.12.

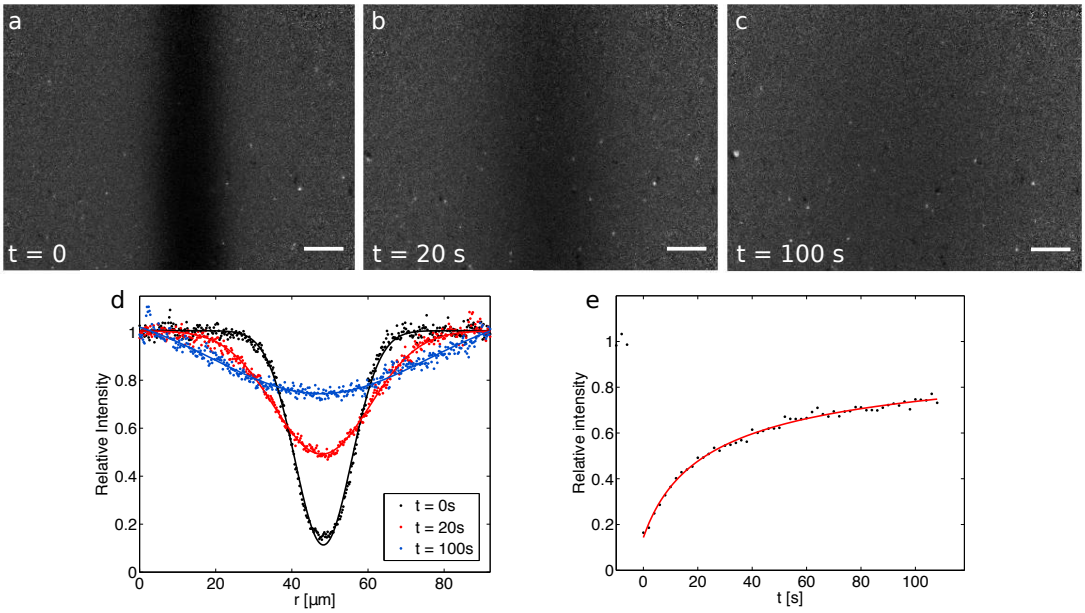

Figure 4.4: *Intensity recovery during a 1D FRAP experiment.* **a**: At $t = 0$, i.e. right after bleaching, the dark rectangle can be clearly discerned. **b**: After 20 seconds, a partial fluorescent recovery is observed within the bleached spot. **c**: The bilayer has recovered almost completely after less than two minutes. However, due to the fraction of immobile molecules, the overall intensity in the middle of the image is still slightly lower than at the edges. The scale bars represent 10 µm. **d**: Line intensity profiles across the slides presented in a-c which show the flattening out of the Gaussian intensity profile over time (solid lines show fits of the data to Eq. 2.8). The minima of the profiles were extracted to constitute the intensity recovery curve. **e**: Intensity recovery over time in a 1D FRAP experiment: data (black dots) and fit to Eq. 2.9 (red solid line) from which the diffusion constant D as well as the fractions of mobile and immobile molecules (F_m and F_{im}, respectively) are determined. It can be seen that the data is well described by the theoretical model.

The diffusion constants and immobile fractions that were obtained for fluorescent SLBs constituted of POPC and *E. coli* lipid extract are summarized in Table 4.1.

Table 4.1: *Diffusion coefficients D and immobile fractions F_{im} obtained from 1D FRAP experiments.*

Lipid	**Cleaning**	D **[µm²/s]**	F_{im} **[%]**
POPC-OG®-DHPE	Piranha	2.02 ± 0.30	8.8 ± 4.5
POPC-OG®-DHPE	acetone	1.50 ± 0.08	9.14 ± 0.53
E. coli extract-OG®-DHPE	ethanol	1.78 ± 0.15	15.91 ± 0.18

POPC Piranha-cleaned: error represents one standard deviation σ from 7 experiments, POPC acetone-cleaned: error represents one standard deviation σ from 3 experiments, *E. coli* lipid extract: error represents one standard deviation σ from 2 experiments

Comparing the results for the POPC SLB on glass slides that were cleaned with different techniques, it can be seen that the lipids diffuse slightly faster on the Piranha-cleaned than on the acetone-cleaned glass slide. Nevertheless, both diffusion constants have the same order of magnitude and are in the spread of values that are expected for a mobile SLB from the literature [48]. It still seems that Piranha-cleaning yields glass slides with less residues. It would then also be expected that less lipids get stuck on the surface due to impurities and consequently that the fraction of mobile molecules is higher. However, the two values for F_{im} agree within their error ranges[2]. It can be concluded that cleaning did indeed affect the diffusivities of the lipids but not considerably.

The diffusion coefficient of the *E. coli* lipids had the same order of magnitude as the values obtained for POPC as well. Interestingly though, the fraction of immobile lipids was higher by almost a factor of 2. Nevertheless, this could be an effect of cleaning. Most importantly for this work, however, was the finding that fluid SLBs could be obtained from *E. coli* lipids with a diffusion constant that was similar to the one from POPC lipids (which was not trivial due to their charge).

Generally, in this thesis I have found several aspects which needed to be considered when performing a FRAP experiment: (I) The bilayer should not be contaminated with unruptured vesicles at the spot that is used for bleaching in order to ensure that the determined intensities are not distorted. (II) Undesirable heavy bleaching over several post-bleach exposures needed to be avoided by using a high filter, e.g. ND 3.0, and a low laser intensity. Otherwise the data was unusable. (III) It turned out to be important to bleach relatively small areas. This is due to the fact that the line intensity profiles across larger bleaching spots could not be properly described by the Gaussian presented in Equation 2.8. Instead, the parameter K, which is a measure for how much bleaching occurs, was overestimated. (IV) If the ratio between bleached and unbleached parts of the SLB was too high in the image to be analyzed, bleaching of the fluorophores during the recovery was overcompensated for[3]. If not considered, both (III) and (IV) consequently resulted in falsified results for the diffusion constants as well as the fraction of immobile molecules.

These problems arose equally for the 2D FRAP experiments. Their results are presented in the following section.

[2]It should be noted though that the high error for F_{im} on the Piranha-cleaned glass slide resulted from experiments with immobile fractions in the ranges of 2% and 4%, which the acetone-cleaned samples did not show.

[3]Another problem with the bleaching compensation for the 1D FRAP experiment as explained in Section 3.5 was that it was assumed that the rate of bleaching changes linearly across the slide without legitimate justification. Considering the results, however, the assumption seemed to be reasonable.

Two-dimensional diffusion of lipids in planar SLBs

The quantitative analysis of two-dimensional FRAP experiments was likewise performed using a custom-written MATLAB script which is presented in Appendix D of this report. Initially, all images needed to be (similarly to the 1D case) normalized using the pre-bleach image in order to account for uneven illumination as well as diffraction artefacts arising from misalignment of the laser.

Afterwards, the images taken during the FRAP experiment (see parts (a)-(d) in Figure 4.5 for examples of three images and their line intensity profiles) could be analyzed regarding the mobility of the lipids. Therefore, the program extracted the integrated intensity within the entire bleached area at every time point in order to obtain a intensity recovery graph (part (e) in Figure 4.5). A fit of this data to Equation 2.11 was then performed in order to obtain the values for D as well as F_{im}.

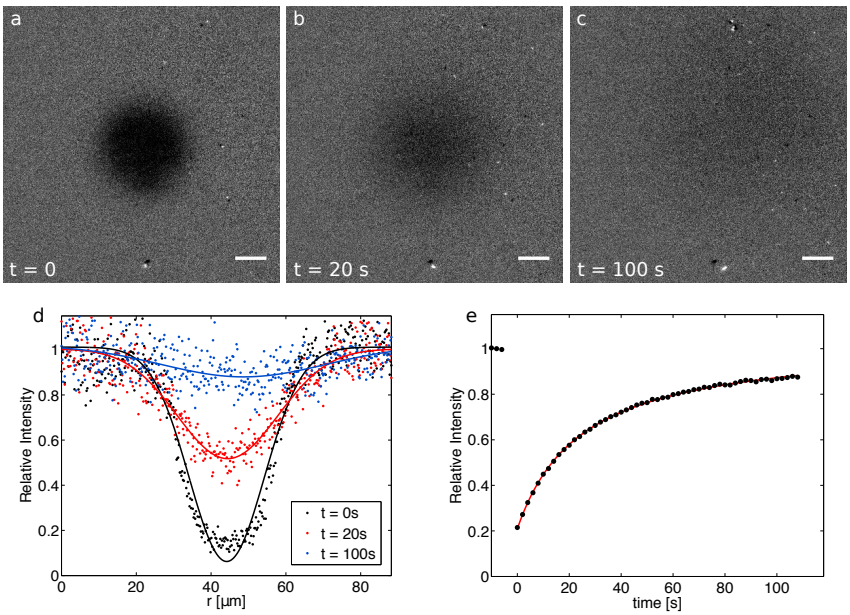

Figure 4.5: *Intensity recovery during a 2D FRAP experiment.* **a**: Immediately after bleaching, the dark circle of photobleached fluorophores can be clearly identified. **b**: After 20 seconds, the intensity has started to recover within the bleached region. **c**: At $t = 100s$ the bleached spot has almost completely recovered. Photobleaching during the exposures of the FRAP experiment resulted in a slight intensity decrease in the upper right of the image. The scale bars indicate 10 µm. **d:** Line intensity profiles across the slide at the different time points depicted in images a-c. The raw data is shown as dots while a fit to Eq. 2.8 of each profile is shown as a solid line in the respective color. Again, the flattening out of the Gaussian over time can be seen. The relatively high spreading of the data can be explained by the low laser intensity (3x times lower than the one used for the data in Figure 4.4) that was used to avoid photobleaching during the experiment. (It should be noted that the line intensity profiles were not needed for the quantitative analysis in a 2D FRAP experiment but are here only shown to further illustrate the intensity recovery.) **e**: Intensity recovery within the entire bleached circle over time in the 2D FRAP experiment: data (black dots) and a fit to Eq. 2.11 (solid red line), which both agree well, are shown. The diffusion constant D as well as the mobile and immobile fractions, F_m and F_{im}, were extracted from this graph.

The diffusion coefficients and immobile fractions that were obtained from 2D FRAP experiments with POPC as well as *E. coli* lipid extract SLBs are presented in Table 4.2. The diffusivity and immobile fraction obtained from the 2D analysis were similar to the values obtained in the 1D case, however, the difference in diffusivity between POPC and *E. coli* lipids was more pronounced in 2D. This was the case even though the 1D and

2D experiments were conducted on the same slide for both *E. coli* and POPC lipids, respectively. This highlights the heterogeneity within the slide. For both types of lipids, all 1D and 2D experiments were each conducted at spots that were relatively close to each other. This can explain why the spreads are low while the averaged diffusivities still differ. Something else to consider is the fact that for the 1D case the bleached area is bigger than for the 2D case. Hence, obstacles on the glass slide have more possibilities to hinder free lipid diffusion. This explains the difference between the diffusion coefficients of POPC obtained with 1D and 2D analysis even though many measurement points were averaged. However, as stated before, all values were in the range expected for fluid SLBs. Hence, both the 1D and 2D analysis gave a similar magnitude on the diffusivity and immobile fraction for similar systems which was important for this work. More detailed experiments are needed in a systematic study to determine the actual difference in diffusivity between E.coli and POPC lipids, but this was beyond the scope of this thesis.

Table 4.2: *Diffusion coefficients D and immobile fractions F_{im} obtained from 2D FRAP experiments.*

Lipid	**Cleaning**	D **[μm²/s]**	F_{im} **[%]**
POPC-OG®-DHPE	Piranha	2.86 ± 0.29	9.5 ± 1.8
E. coli extract-OG®-DHPE	ethanol	1.41 ± 0.09	4.8 ± 3.2

POPC Piranha-cleaned: error represents one standard deviation σ from 6 experiments, *E. coli* lipid extract: error represents one standard deviation σ from 3 experiments

4.2 Lipid bilayers in pipettes

4.2.1 Fluorescence imaging of a lipid-coated pipette

After successfully obtaining planar SLBs, it was also attempted to lipid-coat glass micropipettes in order to obtain a controllable negatively curved SLB that could be used to investigate the membrane binding behavior of DivIVA. The experimental setup from Hernández-Ainsa et al. [32] could not be adopted, because they used a closed system in a PDMS device which would have been too time-consuming to fabricate and also not perfectly suitable for what was supposed to be investigated. Therefore, a protocol for lipid-coating the pipettes that met all requirements set by the intended experiments needed to be established first.

Before the membrane binding experiments could be conducted, the SLBs in pipettes needed to be characterized regarding their mobility as well. Therefore, they were imaged with bright-field as well as epifluorescence microscopy (see Figure 4.6). TIRFM could not be used because the pipette could not be positioned entirely within the evanescent field due to its size. A ring pattern occurred on the fluorescent image due to the diffraction pattern of the laser (which could be avoided by placing a rotating diffuser in the laser beam path or using a non-coherent light source).

Usually, it seemed like the fluorescent image was about 1.5 times smaller than the bright-field one (part (c) in Figure 4.6). It could be argued that this is an indication for the fact that the bilayer only spanned the inside but not the outside of the pipette. However, this would be unexpected, since the outer wall was more readily available for the vesicles to land and form an SLB on. It could also be the case though that the angle of the incoming light as well as the position of the fluorophores let the pipette appear bigger in the bright-field image or simply different focal planes were imaged.

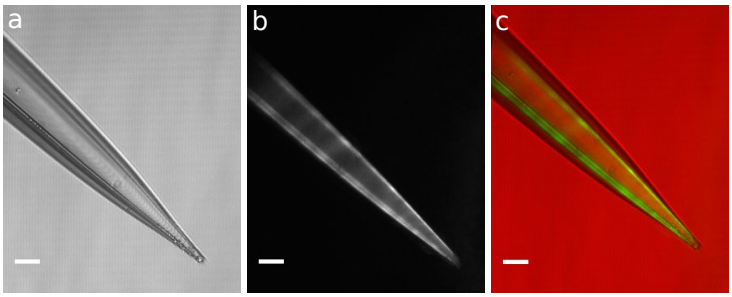

Figure 4.6: *Bright-field (**a**) and fluorescent (**b**) image of a lipid-coated pipette as well as a composite image of the two (**c**).* In the composite image, the red channel shows the bright-field and the green channel the fluorescent image. Used lipids: POPC-OG®-DHPE. The scale bars represent 20 µm.

In order to validate that the lipid-coating resulted in SLBs on the in- as well as the outside wall, a straight, unbent pipette tip after exposure to partially fluorescent lipid vesicles was imaged (see Figure 4.7). It could at least be confirmed that the bilayer spans the inner pipette wall. While there was fluorescent signal on the outside as well, it might have arisen from the part of the inner bilayer that is out of focus due to the conical shape of the pipette tip. The lower intensity in the outermost fluorescent ring also supports this supposition.

A simple photobleaching experiment was performed in the straight pipette as well (see part (c) and (d) in Figure 4.7). It confirmed the fluidity of the bilayer, since the fluorescent intensity recovered.

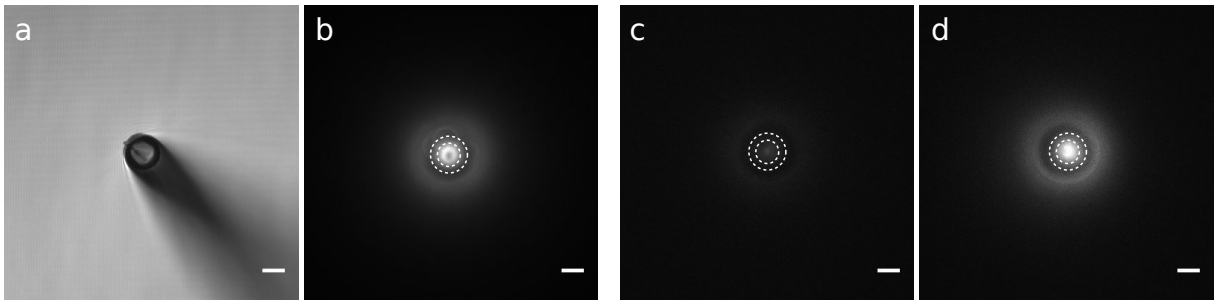

Figure 4.7: *Left*: Bright-field (**a**) and epi-fluorescent (**b**) image of a lipid-coated pipette tip (the image plan is perpendicular to the pipette). *Right*: Results of a qualitative recovery experiment in the straight pipette with an image taken right after bleaching at $t = 0$ (**c**) and 30 minutes later (**d**). The bilayer seems to recover. The dotted circles in b-d represent the inner and outer wall of the pipette, respectively, as seen in a. Used lipids: POPC-OG®-DHPE. All scale bars show 20 µm.

In addition, a negative pressure of -20 kPa was applied to a pipette coated with a fluorescent SLB which was bleached as its tip beforehand (see Figure 4.8).

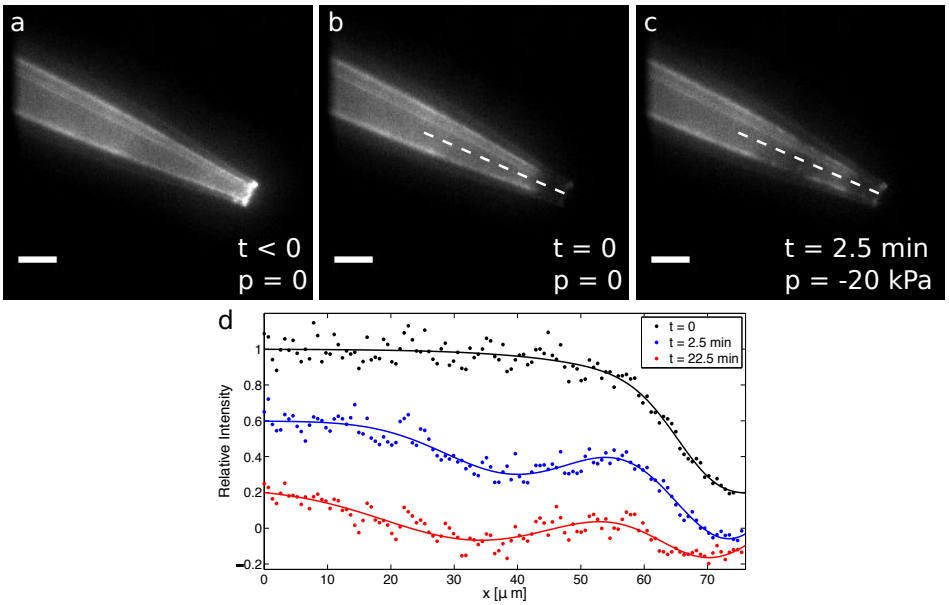

Figure 4.8: *Applying pressure to a lipid-coated micropipette.* **a**: Pre-bleach image of the lipid-coated pipette. **b**: Image of the pipette right after bleaching the tip. **c**: Image of the pipette 2.5 minutes after pressure was applied to it. The photobleached lipids have moved due to the shear forces on the wall induced by the liquid flow such that a second dark area, further away from the pipette tip, has emerged. All scale bars show 20 µm. **d**: Line intensity profiles along the axis of the pipette (as indicated by the white dotted line in b and c) at different time points. Data is shown dotted while fits to Eq. 3.1 are presented as solid lines. The line profiles are spaced apart on the y-axis for reasons of clarity.

Due to the pressure, an inward flow of buffer occured which excerted shear forces on the inner pipette walls and therefore also on the lipid in the SLB. Due to these forces, photobleached lipids moved away from the pipette tip such that another dark region appeared (part (c) in Figure 4.8). This was corroborated when looking at intensity line profiles along the axis of the pipette (part (d) in Figure 4.8). Apart from the intensity minimum from the bleached tip region, another intensity minimum appeared where the photobleached lipids moved to because of the shear forces. Over time, both of these intensity minima recovered due to lipid diffusion. This experiment proved anew that fluid

SLBs were successfully created on the inside of the pipette which was important, since DivIVA was expected to bind to negatively curved lipid bilayers.

Quantitative FRAP experiments were performed as well to determine the diffusion coefficient as well as the immobile fraction of the lipids in the pipette. The results are presented in the subsequent section.

4.2.2 FRAP experiments in a lipid-coated pipette

To assess the diffusion constants as well as immobile and mobile fraction of molecules of the lipid bilayer coating pipette walls, FRAP experiments were conducted in this system as well (see Figure 4.9). The analysis was performed analogously to the 1D FRAP experiment on planar SLBs using a custom-written MATLAB script (presented in Appendix E).

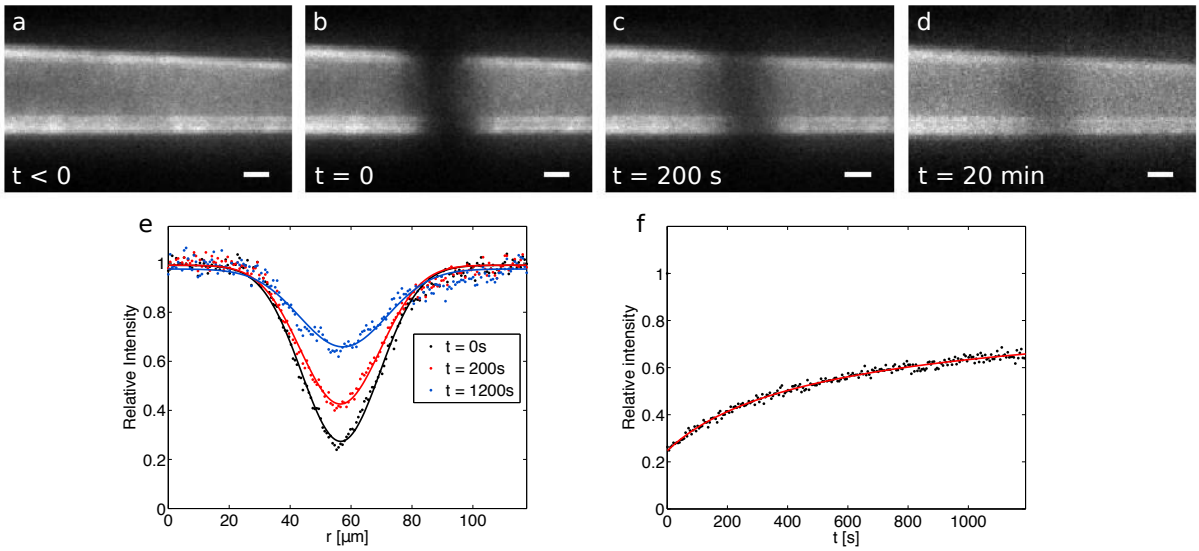

Figure 4.9: *Exemplary 1D FRAP experiment conducted in a pipette coated with a POPC-OG®-DHPE bilayer.* **a**: Pre-bleach image of the pipette. **b**: Image taken right after bleaching at $t = 0$ with a clearly defined photobleached region. **c**: After 200 seconds, a slight intensity increase within the bleached region can be observed. However, the recovery seems much slower in the pipette compared to the planar SLBs (see Figures 4.4 and 4.5). **d**: At $t = 20$ min, the intensity has recovered even more in the bleached area. Nevertheless, the bleached region is still visible suggesting a comparatively high fraction of immobile molecules F_{im}. All scale bars indicate 10 µm. **e**: Line intensity profiles across the slide at the time points depicted in images b-d. The solid lines show a fit of the data (colored dots) to Eq. 2.8. It is again visible here that the intensity minimum clearly increases, however, much less than on planar bilayers. **f**: Intensity recovery in dependence on time in a 1D FRAP experiment in a lipid-coated micropipette. The data is shown as black dots while a fit to Eq. 2.9 is shown as a red line. The recovery is significantly slower and the fraction of immobile molecules higher than on planar lipid bilayers (compare to Figures 4.4 and 4.5.)

Strikingly, the recovery and hence the mobility of the POPC lipids is significantly slower in the pipettes than on the planar lipid bilayers. This can also be seen when comparing the values for the diffusion coefficients in flat SLBs (Table 4.1 and Table 4.2) versus in SLBs in pipettes (Table 4.3). Interestingly, the immobile fractions are also much higher in the pipettes which does not only become evident from the values displayed in Table 4.3 but also from the recovery curve in Figure 4.9 whose final intensity is much lower than the pre-bleach intensity.

Cleaning the pipette with ethanol did not decisively increase the quality of the bilayer (see Table 4.3). Even though the average value of D is higher and the average value of F_{im} is lower, the two values agree within their error ranges. As already stated above for planar bilayers, if the diffusion needs to occur over a longer distance (i.e. if the bleached region is big), the likelihood that the diffusion is slowed down due to residues on the way is increased. It is possible that the cleaning was not thorough enough and that therefore using Piranha solution could increase the mobility (increasing D and lowering F_{im}) of the lipids by removing more obstacles on the walls. Due to time constraints, however, the

experiments could not be repeated with a Piranha-cleaned pipette. This would have been done after pulling and bending the pipette by first fixing it above the Piranha bath such that the solution could be heated, then washing it thoughly with water (taking care that the pipette does not break) and finally blow-drying it under nitrogen flow.

Another possibility is that the lipids being less mobile is just inherent to the curved bilayer because they are sterically hindering each other due to the geometry of the pipette.

Table 4.3: *Diffusion coefficients D and immobile fractions F_{im} obtained from 1D FRAP experiments.*

Lipid	**Cleaning**	D **[μm²/s]**	F_{im} **[%]**
POPC-OG®-DHPE	uncleaned	0.30 ± 0.11	28 ± 10
POPC-OG®-DHPE	ethanol	0.36 ± 0.01	20.6 ± 3.7

All errors represent one standard deviation σ from two experiments.

Generally, conducting a FRAP experiment was more complicated on lipid-coated pipettes than on planar SLBs because the bleached line needed to be perpendicular to the axis of the pipette. Since the pipettes did not occupy the same position during imaging, this required some trials in aligning the FRAP aperture (see microscopy setup in Section 3.2, particularly Figure 3.2).

4.3 Membrane binding of DivIVA

Finally, I used the lipid bilayer systems characterized before, i.e. planar SLBs and lipid-coated pipettes, to investigate the membrane binding behavior of *S. coelicolor* DivIVA *in vitro*. In the following, first the results for DivIVA binding to planar SLBs and afterwards to the curved lipid-coated pipettes are presented.

4.3.1 DivIVA binding to planar membranes

At first, a planar POPC SLB was used to investigate the membrane binding of DivIVA. Since DivIVA was tagged with the protein mNeonGreen and at the time of the experiment the only available fluorescent lipid was OG®-DHPE, both of which were excited using the 488 nm-laser of the microscope, a non-fluorescent POPC bilayer was used.

It was concluded that DivIVA did not bind to the POPC bilayer, since no fluorescence appeared on the surface even 60 minutes after adding DivIVA to the SLB (part (a) in Figure 4.10). To rule out that the protein could not be seen at all with TIRFM, a control experiment was performed. Therefore, the protein was added to a cleaned glass slide that was not coated by an SLB (part (b) in Figure 4.10). In this case, the fluorescence intensity in the TIRF images increased over time as more DivIVA bound to the glass, which could be seen in the intensity development as a function of time (part (c) in Figure 4.10). On the other hand, it did not change during the membrane binding experiment with the POPC bilayer. The inset in part (c) of Figure 4.10 shows the data for the POPC bilayer as well but with a different scale at the y-axis. The intensity did in fact slightly increase soon after adding the protein before it decreased again. Probably, this was due to sporadical DivIVA molecules which bound to defects in the lipid bilayer (at which the glass surface was exposed) but were quickly photobleached. This also suggested that DivIVA was visible once it reached the evanescent field and therefore supported the conclusion that it did not bind to the SLB before.

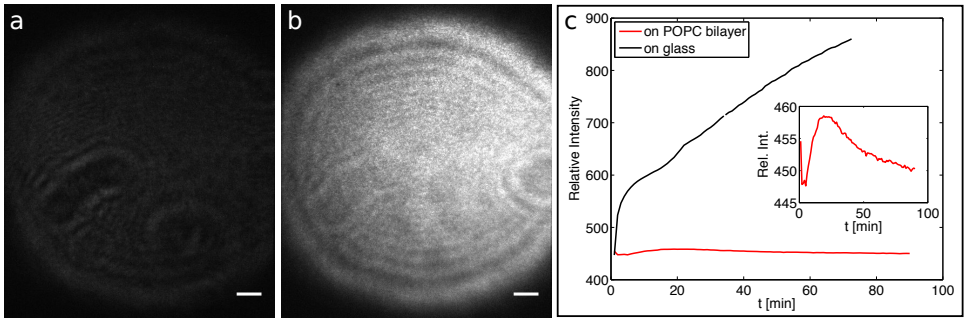

Figure 4.10: *TIRF images of binding of DivIVA to a planar POPC bilayer.* **a**: Picture of a DivIVA binding experiment to a planar (non-fluorescent) POPC bilayer taken 60 minutes after adding the protein. **b**: Picture taken 60 minutes after adding DivIVA to a cleaned glass slide (without any bilayer). Both pictures are presented with the same brightness and contrast settings. **c**: DivIVA binding (represented by the fluorescent intensity of mNeonGreen) onto a POPC bilayer (red line) and a glass slide (black line) as a function of time. The scale bars in a and b indicate 10 µm.

According to the DivIVA membrane binding mechanism proposed by Oliva et al. [50], negative lipids in the membrane stabilize the DivIVA-membrane complex. Considering this, the result that DivIVA did not bind to the POPC bilayer is not surprising, since these lipids are neutrally charged. Consequently, the experiment was repeated with a non-fluorescent bilayer that contained 90% POPC and 10% negatively-charged POPS lipids.

However, the result was the same as for the SLB that consisted exclusively of POPC lipids: no DivIVA bound to the lipid bilayer (see left hand side of Figure 4.11). Since this was rather unexpected, a bleaching experiment was performed to confirm that there was in fact no fluorescent protein present on the POPC/POPS bilayer (see right hand side of Figure 4.11). However, the intensity did not decrease exponentially like in a typical bleaching curve (like the one presented in the inset of part (c) in Figure 4.10), supporting the conclusion that no DivIVA bound even to this negatively-charged SLB.

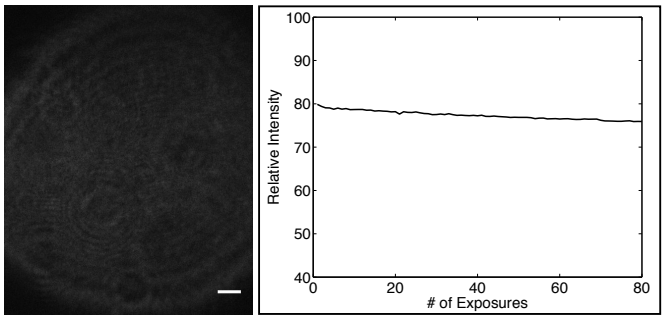

Figure 4.11: *Binding of DivIVA to a POPC/POPS bilayer. Left*: A TIRF image taken 60 minutes after adding DivIVA to a non-fluorescent 9:1 POPC/POPS bilayer. (The image is presented with the same brightness and contrast setting as parts (a) and (b) in Figure 4.10). Scale bar: 10 µm. *Right*: Bleaching experiment of the system, each exposure lasting 100 ms.

A higher percentage of POPS in the bilayer, and the higher negative charge as a consequence thereof, could of course change the membrane binding behavior of DivIVA to some extend. However, these results still indicate that not only the charge but also the type of lipid constituting the SLB might be critical. Since Oliva et al. [50] found that *B. subtilis* DivIVA even binds measurably to liposomes, hence to positively curved membranes, when they are constituted of *E. coli* lipids, the binding experiments were repeated with a planar *E. coli* lipid extract SLB (see Figure 4.12).

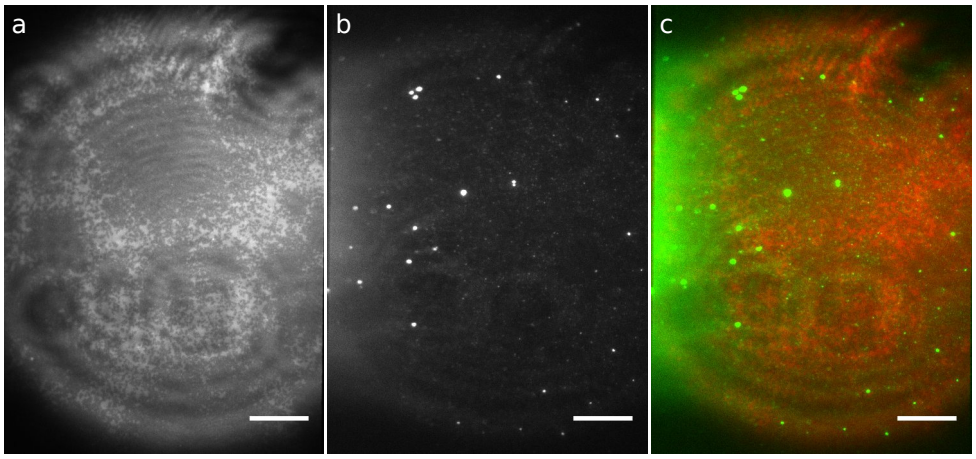

Figure 4.12: *Binding of DivIVA to a planar* E. coli *SLB.* **a**: TIRFM image of an *E. coli* SLB with 0.1 wt% Atto 647N. **b**: TIRFM image of DivIVA binding to the *E. coli* SLB. **c**: Composite image of the *E. coli*-Atto 647N bilayer as excited by the 638 nm laser (red channel) and DivIVA as excited by the 488 nm laser (green channel). All scale bars represent 20 µm.

This time, however, the vesicles were mixed with Atto 647N DHPE such that they could be imaged in the other channel than DivIVA. Since these lipids were not used in our lab before, the successful SLB formation was not trivial. Even though many lipid

vesicles settled on the bilayer without rupturing (white spots in part (a) in Figure 4.12), its fluidity was confirmed with a qualitative FRAP experiment. Afterwards, DivIVA was added to the system. 30 minutes later, fluorescent signal appeared in the 488 nm-channel of the microscope (part (b) of Figure 4.12). It could therefore be concluded that DivIVA had entered the evanescent field. Bright immobile spots probably arose from clustered DivIVA binding to defects in the SLB. Smaller fluorescent spots, however, were diffusing laterally and therefore suggested that DivIVA indeed bound to the *E. coli* lipids. When overlaying fluorescent images from both channels as presented in part (c) of Figure 4.12, the small, mobile spots of protein are much better visible.

To conclude, these experiments confirmed that not only charge but also lipid composition of the bilayer are important for DivIVA membrane binding. The role of curvature was to be investigated thereafter.

4.3.2 DivIVA binding to negatively curved membranes

Finally, it was investigated how DivIVA binds to POPC bilayers in pipettes. Again, the SLBs were non-fluorescent. After lipid-coating, the pipettes were exposed to *S. coelicolor* DivIVA and finally imaged with bright-field and epifluorescence microscopy (see parts (a) and (b) in Figure 4.13). As a control trial, the experiment was also repeated with a non-coated glass pipette (part (c) in Figure 4.13).

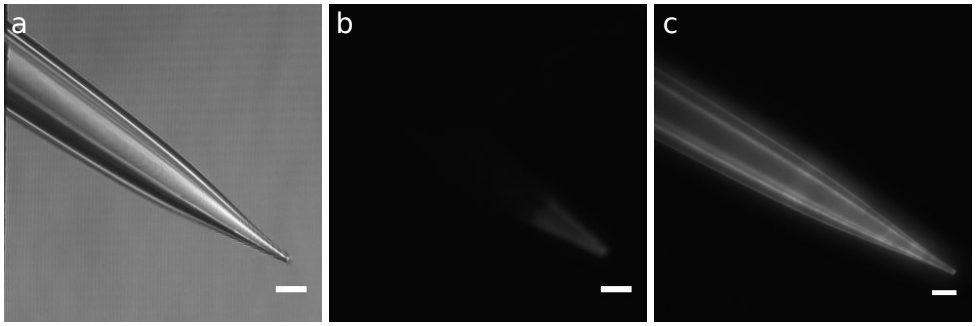

Figure 4.13: *Binding of DivIVA to a POPC bilayer coating a micropipette compared to an uncoated pipette.* **a**: Bright-field image of the pipette (coated with a non-fluorescent POPC bilayer) that was used for the DivIVA membrane binding experiment. **b**: Fluorescent image of the same pipette. At the pipette tip, some fluorescent DivIVA has bound. **c**: Fluorescent image of a pipette that was exposed to fluorescently-labeled DivIVA without prior lipid coating. The fluorescent images in b and c are presented with the same brightness and contrast settings for better comparison. The scale bars represent 20 μm.

As expected, the whole pipette was illuminated when no lipid-coating was performed, as the fluorescent protein binds everywhere to the glass, similarly to the results presented for the binding of DivIVA to a planar glass surface in part (b) of Figure 4.10. Interestingly, in the lipid-coated pipette, on the other hand, only the tip region showed fluorescent signal. At first it was believed that this confirmed that it can be shown also in an IN VITRO membrane model system that DivIVA preferably binds to negative curvature. However, the fluorescent area has a very sharp edge which is rather unexpected. Furthermore, the pipette has a diameter of approximately 20 μm at the upper end of this region. This is significantly bigger than the diameter of bacterial cells (≈ 1 μm) in which DivIVA tends to localize to the parts of the cell membrane with highest negative curvature. This does not necessarily mean that DivIVA does not bind to very low negative curvatures, however, it seems unlikely since no binding at all was observed on the planar SLBs. Another indication that the protein in fact did not bind to the POPC bilayer is presented in Figure 4.14. The fluorophores at the tip of the pipette were photobleached. If the protein had actually been bound to an SLB, it would have been expected that the fluorescent intensity recovers as the lipids diffuse around (similarly to what was found on the flat *E. coli* bilayer, see Figure 4.12). However, this was not the case. Therefore, it was concluded that DivIVA did not bind to the lipids but that the SLB had not properly formed, leaving glass exposed for the protein to stick to.

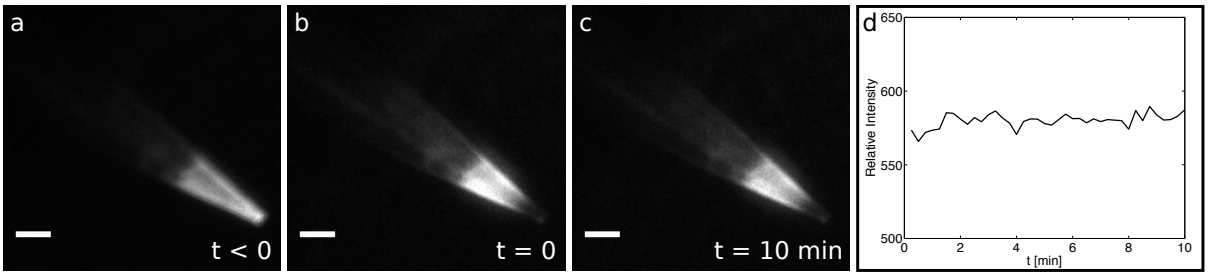

Figure 4.14: *Bleaching experiment of DivIVA bound to a pipette that was lipid-coated with POPC (the same as shown in Figure 4.13).* **a**: Pre-bleach image of the lipid-coated pipette that was exposed to fluorescently-labeled DivIVA. **b**: Fluorescent image of the pipette right after the DivIVA was bleached at its tip. **c**: After 10 minutes, the bleached region is still clearly visible. **d**: The intensity development over time in the bleached tip. Evidently, no intensity recovery occured. The scale bars in a-c indicate 20 μm.

The experiment was repeated two more times (bright-field and fluorescent images presented in Figure 4.15). However, the results from the first trial could not be reproduced. Instead it seems that in the first repetition, the SLB had not formed properly, since the whole pipette was illuminated. To test this, a bleaching experiment (similar to the one presented in Figure 4.14) was conducted as well. However, due to the very low fluorescence intensity, the data was not utilizable. In the second trial, DivIVA localized indeed preferably to the tip region. However, it cannot be validated that this was due to the curvature of the bilayer, but rather seems like it bound to obstacles on the walls. These experiments elucidate again the importance of using fluorescent bilayers for membrane binding studies.

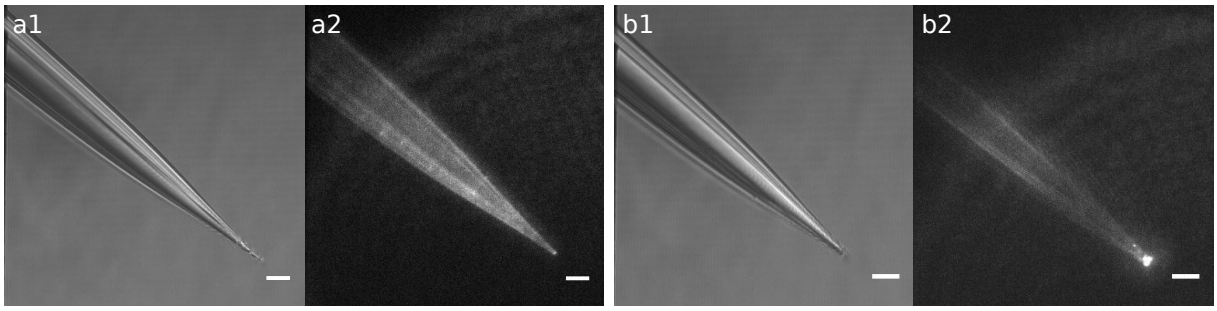

Figure 4.15: *Reiterations of the experiment to observe DivIVA binding to a micropipette that was coated with a POPC bilayer.* Bright-field (a1 and b1) and fluorescent images (a2 and b2, both presented with the same brightness and contrast settings) of pipettes that were first lipid-coated with POPC and subsequently exposed to fluorescently-labeled DivIVA. Scale bars: 20 μm.

All in all, it seems that DivIVA did not accumulate in the POPC bilayer under these conditions. This is not surprising considering that the lipid composition already showed important for DivIVA binding on flat SLBs.

Nevertheless, this work showed that utilizing a lipid-coated pipette as model system for curved membranes is possible. The protocol for the coating process was established and can be easily modified to use different kinds lipid. In the case of DivIVA it would be interesting to see how the results change when POPS or *E. coli* lipid extract are used to shed more light on the role of charge, lipid composition and curvature in the DivIVA membrane binding mechanism. Furthermore, the experimental protocol can also be used for coating pipettes with diameters in the nm-range. The curvatures in their tips would more closely resemble what is found in the bacterial cells naturally containing DivIVA.

Chapter 5

Conclusions and Outlook

To summarize, during this thesis work fluid lipid bilayers on planar surfaces as well as in glass micropipettes were successfully obtained. Custom-written MATLAB scripts were used to quantify the mobility of the lipids in both systems. The diffusivities on flat SLBs did not vary significantly between different types of lipids or cleaning techniques used. However, a much lower mobility of lipids was found in SLBs spanning micropipettes. Cleaning could be a problem here as well, but this property might also be inherent to the curved lipid bilayer. A question that remained was if the bilayer forms on the in- as well as the outside of the pipette which was tried to be assessed by imaging a straight pipette. Repeating this experiment using confocal microscopy (which offers much higher optical resolution and contrast because all fluorescence from outside of the focal plane is eliminated), could ascertain whether the lipid bilayer forms on both sides of the pipette walls. It would be also interesting to see in how far shear forces act on the pipette walls if a flow is applied to the pipette (which was already shown possible in this work). This could be done by determining the velocity of the movement of the bleached spot as the flow prevails. Simulations of the flow in COMSOL MULTIPHYSICS® could then be compared to the experimentally obtained values.

Moreover, the binding of the protein DivIVA to both membrane model systems was investigated. It was found that DivIVA binds to and diffuses within planar SLBs consisting of *E. coli* lipids, but not when they consist of neutrally-charged POPC or negatively-charged POPS lipids. This illustrated that not only charge but also lipid composition are important for the membrane binding process. It was furthermore found that DivIVA did not bind to curved POPC bilayers. However, a major drawback of the setup used for most of the DivIVA membrane binding experiments was that the SLB was non-fluorescent. This gave no opportunity to examine if the lipid bilayers had formed properly and how mobile they were. These experiments should therefore be repeated with lipids like Atto 647N DHPE as fluorescent markers, since they could be excited with the 638 nm laser in the microscope. Nevertheless, a protocol for lipid-coating glass pipettes and therefore obtaining a model system of the curved cell membrane was successfully established and can be easily modified for using different types of lipids and pipettes with smaller diameters (e.g. in the nm-range). Naturally, the use of the lipid-coated pipette could not only be used to investigate DivIVA, but also the membrane binding behavior of other proteins, like e.g. α-synuclein which is associated with Parkinson's disease. However, in this case it would be beneficial to restrict the bilayer to only form on the inside *or* the outside of the pipette to be able to distinguish between binding to positive and to negative curvature. This could be achieved by coating the glass in- or outside with a material that SLBs are

known to not form on. It is also possible (even though challenging) to fill the pipette with the lipid vesicle solution to ensure that a bilayer only forms on the inside.

The lipid-coated glass pipette as presented in this work might not only be interesting to investigate the membrane binding behavior of proteins but could also be used for other purposes. It was shown before that lipid-coating prevents sticking of proteins to the walls of microfluidic devices [57]. Therefore, a lipid-coating could for example significantly improve the quality of delivery experiments to surfaces, since it could prevent sticking of the molecules to and ultimately clogging of the pipette.

Acknowledgments

Foremost, my gratitude goes to my supervisors Jonas Tegenfeldt and especially Peter Jönsson for providing me with the opportunity to perform this thesis work. Peter has been the most approachable and dedicated supervisor I have ever encountered and is largely responsible for the knowledge I have gained since October. I greatly value how much freedom he gave me with this project while always being readily available when I needed guidance and support (or comments on my thesis draft within a few hours).

Furthermore, I want to thank Klas Flärdh and Algirdas from the Biology department, not only for expressing DivIVA but also for insightful interdisciplinary meetings and discussions which taught me a lot. I hope I can give back some interesting results in return.

Not to forget, I want to thank Vicky of course for the all-time support, countless ideas and input she has given me during the last two semesters and the time she has put into revising this text (!). I don't think she can imagine how much I appreciated the occasional distracting Denglish chitchat and laughter about "Gott und die Welt", especially in the last couple of weeks during which I was struggling quite a bit.

Additionally, I would like to thank everyone working at the Physical Chemistry department for creating this incredibly organized and uniquely social working environment. I will always remember one or the other talk or lunch discussion and hope I can establish the traditions of fruit baskets and Friday cake wherever I go.

In particular, my warm gratitude goes to Maria - a.k.a. best office mate, Spanish teacher and chocolate provider one can wish for. She has made me feel so welcomed and appreciated, listened to everything, work-related or not, that I needed to get out. ¡Me gusta la montaña, me gustas tú!

I would also like to mention my friends Nadine, Regina and Sae as well as Erik (whose friend I will hopefully be one day) who helped and supported me way more than they think or get credit for with this short sentence.

Last but definitely not least, my thanks are directed to my entire great and wonderful family. Gerade in den letzten Monaten, und insbesondere dieses Wochenende, habe ich gemerkt, was für ein Geschenk es ist Euren Rückhalt zu haben. Weder diese Arbeit noch alles was war oder noch kommen wird, hätte ich ohne Eure Unterstützung so umsetzen können. Dafür bin ich unendlich dankbar.

References

[1] S. J. Singer and G. L. Nicolson. The Fluid Mosaic Model of the Structure of Cell Membranes. *Science*, 175(4023):720–731, 1972.

[2] P. Mueller, D. O. Rudin, H. Ti Tien, and W. C. Wescott. Reconstitution of Cell Membrane Structure In Vitro and Its Transformation into an Excitable System. *Nature*, 194:979–980, 1962.

[3] L. K. Tamm and H. M. McConnell. Supported phospholipid bilayers. *Biophysical Journal*, 47(1):105, 1985.

[4] E. T. Castellana and P. S. Cremer. Solid supported lipid bilayers: From biophysical studies to sensor design. *Surface Science Reports*, 61(10):429–444, 2006.

[5] R. P. Richter, J. Lai Kee Him, and A. Brisson. Supported Lipid Membranes. *Materials Today*, 6(11):32–37, 2003.

[6] M. Grandbois, H. Clausen-Schaumann, and H. Gaub. Atomic Force Microscope Imaging of Phospholipid Bilayer Degradation by Phospholipase A2. *Biophysical Journal*, 74(5):2398–2404, 1998.

[7] V. T. Chang, R. A. Fernandes, K. A. Ganzinger, S. F. Lee, C. Siebold, J. McColl, P. Jönsson, M. Palayret, K. Harlos, C. H. Coles, et al. Initiation of T Cell Signaling by CD45 Segregation at 'Close Contacts'. *Nature Immunology*, 2016.

[8] T. Baumgart, B. R. Capraro, C. Zhu, and S. L. Das. Thermodynamics and Mechanics of Membrane Curvature Generation and Sensing by Proteins and Lipids. *Changes*, 29(6):997–1003, 2012.

[9] J. Zimmerberg and M. M. Kozlov. How Proteins Produce Cellular Membrane Curvature. *Nature Reviews Molecular Cell Biology*, 7(1):9–19, 2006.

[10] B. J. Peter, H. M. Kent, I. G. Mills, Y. Vallis, P. J. G. Butler, P. R. Evans, and H. T. McMahon. BAR Domains as Sensors of Membrane Curvature: The Amphiphysin BAR Structure. *Science*, 303(5657):495–499, 2004.

[11] A. Frost, V. M. Unger, and P. De Camilli. The bar domain superfamily: Membrane-molding macromolecules. *Cell*, 137(2):191–196, 2009.

[12] S. S. Y. Chong, S. G. Taneva, J. M. C. Lee, and R. B. Cornell. The Curvature Sensitivity of a Membrane-Binding Amphipathic Helix Can Be Modulated by the Charge on a Flanking Region. *Biochemistry*, 53(3):450–61, 2014.

[13] R. Lenarcic, S. Halbedel, L. Visser, M. Shaw, L. J. Wu, J. Errington, D. Marenduzzo, and L. W. Hamoen. Localisation of DivIVA by targeting to negatively curved membranes. *The EMBO Journal*, 28(15):2272–2282, 2009.

[14] H. Stahlberg, E. Kutejová, K. Muchová, M. Gregorini, A. Lustig, S. A. Müller, V. Olivieri, A. Engel, A. J. Wilkinson, and I. Barák. Oligomeric structure of the Bacillus subtilis cell division protein DivIVA determined by transmission electron microscopy. *Molecular Microbiology*, 52(5):1281–1290, 2004.

[15] D. H. Edwards and J. Errington. The Bacillus Subtilis DivIVA Protein Targets to the Division Septum and Controls the Site Specificity of Cell Division. *Molecular Microbiology*, 24(5):905–915, 1997.

[16] A. L. Marston, H. B. Thomaides, D. H. Edwards, M. E. Sharpe, and J. Errington. Polar Localization of the MinD Protein of Bacillus Subtilis and Its Role in Selection of the Mid-Cell Division Site. *Genes & Development*, 12(21):3419–3430, 1998.

[17] L. D. Renner, P. Eswaramoorthy, K. S. Ramamurthi, and D. B. Weibel. Studying Biomolecule Localization by Engineering Bacterial Cell Wall Curvature. *PLoS ONE*, 8(12):e84143, 2013.

[18] A. Tian and T. Baumgart. Sorting of Lipids and Proteins in Membrane Curvature Gradients. *Biophysical Journal*, 96(7):2676–2688, 2009.

[19] B. R. Capraro, Y. Yoon, W. Cho, and T. Baumgart. Curvature Sensing by the Epsin N-Terminal Homology Domain Measured on Cylindrical Lipid Membrane Tethers. *Journal of the American Chemical Society*, 132(4):1200–1201, 2010.

[20] C. Prévost, H. Zhao, J. Manzi, E. Lemichez, P. Lappalainen, A. Callan-Jones, and P. Bassereau. IRSp53 Senses Negative Membrane Curvature and Phase Separates along Membrane Tubules. *Nature Communications*, 6, 2015.

[21] X. Jiang, S. Takayama, X. Qian, E. Ostuni, H. Wu, N. Bowden, P. LeDuc, D. E. Ingber, and G. M. Whitesides. Controlling Mammalian Cell Spreading and Cytoskeletal Arrangement with Conveniently Fabricated Continuous Wavy Features on Poly(dimethylsiloxane). *Langmuir*, 18(8):3273–3280, 2002.

[22] W.-T. Hsieh, C.-J. Hsu, B. R. Capraro, T. Wu, C.-M. Chen, S. Yang, and T. Baumgart. Curvature Sorting of Peripheral Proteins on Solid-Supported Wavy Membranes. *Langmuir*, 28(35):12838–12843, 2012.

[23] K. Zieske, J. Schweizer, and P. Schwille. Surface Topology Assisted Alignment of Min Protein Waves. *FEBS Letters*, 588(15):2545–2549, 2014.

[24] A. P. Dabkowska, C. S. Niman, G. Piret, H. Persson, H. P. Wacklin, H. Linke, C. N. Prinz, and T. Nylander. Fluid and Highly Curved Model Membranes on Vertical Nanowire Arrays. *Nano Letters*, 14(8):4286–4292, 2014.

[25] T. Takami, B. H. Park, and T. Kawai. Nanopipette exploring nanoworld. *Nano Convergence*, 1(1):17, 2014.

[26] A. Bruckbauer, P. James, D. Zhou, J. W. Yoon, D. Excell, Y. Korchev, R. Jones, and D. Klenerman. Nanopipette Delivery of Individual Molecules to Cellular Compartments for Single-Molecule Fluorescence Tracking. *Biophysical Journal*, 93(9):3120–3131, 2007.

[27] B. Babakinejad, P. Jönsson, A. López Córdoba, P. Actis, P. Novak, Y. Takahashi, A. Shevchuk, U. Anand, P. Anand, A. Drews, A. Ferrer-Montiel, D. Klenerman, and Y. E. Korchev. Local Delivery of Molecules from a Nanopipette for Quantitative Receptor Mapping on Live Cells. *Analytical Chemistry*, 85(19):9333–9342, 2013.

[28] J. D. Piper, R. W. Clarke, Y. E. Korchev, L. Ying, and D. Klenerman. A Renewable Nanosensor Based on a Glass Nanopipette. *Journal of the American Chemical Society*, 128(51):16462–16463, 2006.

[29] G. Stober, L. J. Steinbock, and U. F. Keyser. Modeling of Colloidal Transport in Capillaries. *Journal of Applied Physics*, 105(8):084702, 2009.

[30] N. A. W. Bell, V. V. Thacker, S. Hernández-Ainsa, M. E. Fuentes-Perez, F. Moreno-Herrero, T. Liedl, and U. F. Keyser. Multiplexed Ionic Current Sensing with Glass Nanopores. *Lab on a Chip*, 13(10):1859, 2013.

[31] Allen J Bard, Fu Ren F Fan, Juhyoun Kwak, and Ovadia Lev. Scanning Electrochemical Microscopy. Introduction and Principles. *Analytical Chemistry*, 61(2):132–138, 1989.

[32] S. Hernández-ainsa, C. Muus, Nicholas A. W. Bell, and L. J. Steinbock. Supporting information to : Contents :. 2012.

[33] H. M. McConnell, T. H. Watts, R. M. Weis, and A. A. Brian. Supported planar membranes in studies of cell-cell recognition in the immune system. *Biochimica et Biophysica Acta (BBA)-Reviews on Biomembranes*, 864(1):95–106, 1986.

[34] E. Reimhult, B. Kasemo, and F. Höök. Rupture pathway of phosphatidylcholine liposomes on silicon dioxide. *International Journal of Molecular Sciences*, 10(4):1683–1696, 2009.

[35] S. J. Johnson, T. M. Bayerl, D. C. McDermott, G. W. Adam, A. R. Rennie, R. K. Thomas, and E. Sackmann. Structure of an adsorbed dimyristoylphosphatidylcholine bilayer measured with specular reflection of neutrons. *Biophysical Journal*, 59(2):289, 1991.

[36] S. Hernández-Ainsa, C. Muus, N. A. W. Bell, L. J. Steinbock, V. V. Thacker, and U. F. Keyser. Lipid-coated nanocapillaries for DNA sensing. *The Analyst*, 138(1):104–106, 2013.

[37] D. Axelrod, T. P. Burghardt, and N. L. Thompson. Total internal reflection fluorescence. *Annual Review of Biophysics and Bioengineering*, 13(1):247–268, 1984.

[38] D. Axelrod. Total internal reflection fluorescence microscopy in cell biology. *Traffic*, 2(11):764–774, 2001.

[39] D. Axelrod, D. E. Koppel, J. Schlessinger, E. Elson, and W. W. Webb. Mobility measurement by analysis of fluorescence photobleaching recovery kinetics. *Biophysical Journal*, 16(9):1055, 1976.

[40] T. K. L. Meyvis, S. C. De Smedt, P. Van Oostveldt, and J. Demeester. Fluorescence Recovery After Photobleaching: A Versatile Tool for Mobility and Interaction Measurements in Pharmaceutical Research. *Pharmaceutical Research*, 16(8):1153–1162, 1999.

[41] E. A. J. Reits and J. J. Neefjes. From fixed to FRAP: measuring protein mobility and activity in living cells. *Nature Cell Biology*, 3(6):E145–E147, 2001.

[42] B. L. Sprague, R. L. Pego, D. A. Stavreva, and J. G. McNally. Analysis of Binding Reactions by Fluorescence Recovery After Photobleaching. *Biophysical Journal*, 86(6):3473–3495, 2004.

[43] A. Einstein. Über die von der molekularkinetischen Theorie der Wärme geforderte Bewegung von in ruhenden Flüssigkeiten suspendierten Teilchen. *Annalen der Physik*, 322(8):549–560, 1905.

[44] R. B. Bird. Transport phenomena. *Applied Mechanics Reviews*, 55(1):R1–R4, 2002.

[45] A. Fick. Ueber Diffusion. *Annalen der Physik*, 170(1):59–86, 1855.

[46] B. Johansson, F. Höök, D. Klenerman, and P. Jönsson. Label-Free Measurements of the Diffusivity of Molecules in Lipid Membranes. *ChemPhysChem*, 15(3):486–491, 2014.

[47] P. Jönsson and B. Jönsson. Hydrodynamic Forces on Macromolecules Protruding from Lipid Bilayers due to External Liquid Flows. *Langmuir*, 31(46):12708–12718, 2015.

[48] P. Jönsson, M. P. Jonsson, J. O. Tegenfeldt, and F. Höök. A Method Improving the Accuracy of Fluorescence Recovery After Photobleaching Analysis. *Biophysical Journal*, 95(11):5334–5348, 2008.

[49] D. Claus. A Standardized Gram Staining Procedure. *World Journal of Microbiology and Biotechnology*, 8(4):451–452, 1992.

[50] M. A. Oliva, S. Halbedel, S. M. Freund, P. Dutow, T. A. Leonard, D. B. Veprintsev, L. W. Hamoen, and J. Löwe. Features critical for membrane binding revealed by DivIVA crystal structure. *The EMBO Journal*, 29(12):1988–2001, 2010.

[51] W. Humphrey, A. Dalke, and K. Schulten. Vmd: visual molecular dynamics. *Journal of Molecular Graphics*, 14(1):33–38, 1996.

[52] K. Flärdh. Essential role of DivIVA in polar growth and morphogenesis in Streptomyces coelicolor A3(2). *Molecular Microbiology*, 49(6):1523–1536, 2003.

[53] A. M. Hempel, S. Cantlay, V. Molle, S.-B. Wang, M. J. Naldrett, J. L. Parker, D. M. Richards, Y.-G. Jung, M. J. Buttner, and K. Flärdh. The Ser/Thr protein kinase AfsK regulates polar growth and hyphal branching in the filamentous bacteria *Streptomyces*. *Proceedings of the National Academy of Sciences*, 109(35):E2371–E2379, 2012.

[54] Avanti Polar Lipids. Phospholipids Product Information, `https://avantilipids.com/product-category/products/phospholipids/`, accessed on 03/31/2016.

[55] Jmol: an open-source Java viewer for chemical structures in 3D, `http://www.jmol.org/`, downloaded on 03/30/2016.

[56] S. Chong, F. B. Mersha, D. G. Comb, M. E. Scott, D. Landry, L. M. Vence, F. B. Perler, J. Benner, R. B. Kucera, C. A. Hirvonen, et al. Single-Column Purification of Free Recombinant Proteins Using a Self-Cleavable Affinity Tag Derived From a Protein Splicing Element. *Gene*, 192(2):271–281, 1997.

[57] F. Persson, J. Fritzsche, K. U. Mir, M. Modesti, F. Westerlund, and J. O. Tegenfeldt. Lipid-Based Passivation in Nanofluidics. *Nano Letters*, 12(5):2260–5, 2012.

Appendices

Appendix A

Derivation of 1D intensity recovery equation

We are trying to solve Fick's second law (the diffusion equation)

$$\frac{\partial c}{\partial t} = D\frac{\partial^2 c}{\partial x^2} \qquad \text{for } \; x \in \mathbb{R},\; t > 0 \tag{A.1}$$

for bleaching a line in order to extract the one-dimensional diffusion constant. As initial conditions we require:

$$c(x, t = 0) = I_I \left(1 - K \exp\left(\frac{-(x-b)^2}{w^2}\right)\right). \tag{A.2}$$

It furthermore holds that $c(x, t \to \infty) = I_I$. However, we need our function to go to 0 as $t \to \infty$ to simplify solving the equations. Hence, we use a variable substitution:

$$u(x, t) = I_I - c(x, t) \tag{A.3}$$

$$u(x, t = 0) = I_I K \exp\left(\frac{-(x-b)^2}{w^2}\right). \tag{A.4}$$

For simplicity reasons we will subtitute $x' = x - b$. The goal is now to find a $u(x', t)$ that fulfills Fick's second law. Therefore, we start with applying the Fourier transform with respect to x' ($\mathcal{F}_{x'}$) to Equation A.1. Since we only derivate with respect to time on the left-hand side this simply becomes:

$$\frac{\partial \hat{u}(k, t)}{\partial t}, \tag{A.5}$$

where

$$\hat{u}(k, t) = \mathcal{F}_{x'} u(k, t) = \int_{-\infty}^{\infty} e^{-ikx'} u(x', t) dx', \tag{A.6}$$

while on the right-hand side the following is obtained:

$$(ik)^2 \hat{u}(k, t) = -k^2 \hat{u}(k, t). \tag{A.7}$$

Plugging back into Equation A.1 we get the partial differential Equation

$$\frac{\partial \hat{u}(k, t)}{\partial t} = -Dk^2 \hat{u}(k, t) \tag{A.8}$$

which has the solution

$$\hat{u}(k,t) = const(k) \cdot e^{-Dk^2t} \tag{A.9}$$

for which the constant $const(k) = \hat{u}(k, t = 0)$ needs to be determined.

$$\hat{u}(k,t=0) = \mathcal{F}_{x'}u(k,t=0) \tag{A.10}$$
$$= \int_{-\infty}^{\infty} e^{-ikx'}u(x',t=0)dx' \tag{A.11}$$
$$= \int_{-\infty}^{\infty} e^{-ikx'}I_I K e^{-x'^2/w^2}dx' \tag{A.12}$$

and using $\int_{-\infty}^{\infty} e^{-ikx'}e^{-\alpha x'^2} = \sqrt{\pi/\alpha} \cdot \exp(-k^2/(4\alpha))$ yields then for $\hat{u}(k,t)$:

$$\hat{u}(k,t) = I_I K\sqrt{w^2\pi} \cdot e^{-k^2w^2/4} \cdot e^{-Dk^2t}. \tag{A.13}$$

In order to obtain $u(x,t)$ and consequently $c(x,t)$, the inverse Fourier transform $\mathcal{F}_k^{-1}$ needs to be applied to $\hat{u}(k,t)$:

$$\mathcal{F}_k^{-1}u(x',t) = \frac{1}{2\pi}\int_{-\infty}^{\infty} e^{ikx'}\hat{u}(k,t)dk \tag{A.14}$$
$$= \frac{1}{2\pi}\mathcal{F}_k\hat{u}(k,-t), \quad \text{with } \epsilon = -x' \tag{A.15}$$
$$= \frac{1}{2\pi}\int_{-\infty}^{\infty} e^{-ik\epsilon} \cdot I_I K\sqrt{w^2\pi} \cdot e^{-k^2w^2/4} \cdot e^{-Dk^2t}dk. \tag{A.16}$$

Using the same identity as before as well as resubstituting $\epsilon = -x'$ yields:

$$u(x',t) = \frac{1}{2\pi}I_I K\sqrt{w^2\pi}\sqrt{\frac{\pi}{w^2/4 + Dt}} \cdot e^{-x'^2/(w^2+4Dt)} \tag{A.17}$$
$$= I_I K\sqrt{\frac{w^2}{w^2+4Dt}} \cdot e^{-x'^2/(w^2+4Dt)}, \tag{A.18}$$

which means we finally get for $c(x,t)$:

$$c(x,t) = I_I - u(x,t) \tag{A.19}$$
$$= I_I\left(1 - K\sqrt{\frac{w^2}{w^2+4Dt}} \cdot \exp\frac{-(x-b)^2}{(w^2+4Dt)}\right). \tag{A.20}$$

Evaluating the equation above at the middle of the bleached region (hence at $x = b$) gives:

$$c(t) = I_I\left(1 - K\sqrt{\frac{w^2}{w^2+4Dt}}\right), \tag{A.21}$$

which is exactly the same as Equation 2.9 (before incorporating the term for the immobile fraction).

Appendix B

Derivation of 2D intensity recovery equation

The derivation is in principle the same as in Appendix A just that now a solution to Fick's law in two dimensions:

$$\frac{\partial c}{\partial t} = D(\frac{\partial^2 c}{\partial x^2} + \frac{\partial^2 c}{\partial x^2}) \tag{B.1}$$

with the following initial condition

$$c(x, y, t = 0) = I_I \left(1 - K \exp\left(-\frac{(x - b_1)^2 + (y - b_2)^2}{w^2}\right)\right) \tag{B.2}$$

and boundary condition

$$c(x, y, t \to \infty) = I_I \tag{B.3}$$

needs to be found. For the same reasons as before, we will use $x' = x - b_1$, $y' = y - b_2$ and $u(x', y', t) = I_I - c(x', y', t)$. By using the 2D Fourier transform of $u(x, y, t)$

$$\hat{u}(k_x, k_y, t) = \mathcal{F}_{x,y} u(k_x, k_y, t) = \int_{-\infty}^{\infty}\int_{-\infty}^{\infty} e^{-ik_x x'} e^{-ik_y y'} u(x', y', t) dx' dy' \tag{B.4}$$

Equation B.1 becomes:

$$\frac{\partial \hat{u}(k_x, k_y, t)}{\partial t} = -D(k_x^2 + k_y^2) \cdot \hat{u}(k_x, k_y, t). \tag{B.5}$$

Similarly to the 1D case, Equation B.5 has the solution

$$\hat{u}(k_x, k_y, t) = const(k_x, k_y) \cdot \exp\left(-D(k_x^2 + k_y^2)t\right), \tag{B.6}$$

where $const(k_x, k_y) = \hat{u}(k_x, k_y, t = 0)$ is determined as before:

$$\hat{u}(k_x, k_y, t = 0) = \mathcal{F}_{x',y'} u(k_x, k_y, t = 0) \tag{B.7}$$

$$= \int_{-\infty}^{\infty}\int_{-\infty}^{\infty} e^{-ik_x x'} e^{-ik_y y'} I_I K \exp\left(-\frac{x'^2 + y'^2}{w^2}\right) dx' dy' \tag{B.8}$$

$$= I_I K \int_{-\infty}^{\infty} e^{-ik_x x'} \exp\left(-\frac{x'^2}{w^2}\right) dx' \int_{-\infty}^{\infty} e^{-ik_y y'} \exp\left(-\frac{y'^2}{w^2}\right) dy' \tag{B.9}$$

$$= I_I K w^2 \pi \exp\left(-\frac{w^2}{4}(k_x^2 + k_y^2)\right), \tag{B.10}$$

where in the last step again $\int_{-\infty}^{\infty} e^{-ikx'} e^{-\alpha x'^2} = \sqrt{\pi/\alpha} \cdot \exp(-k^2/(4\alpha))$ was used. Finally, the 2D inverse Fourier transform $\mathcal{F}^{-1}_{x',y'}$ can be applied to obtain $u(x', y', t)$ (using $\epsilon_x = -x'$ and $\epsilon_y = -y'$ in the second and resubstituting in the last step):

$$u(x', y', t) = \mathcal{F}^{-1}_{k_x,k_y} u(x', y', t) \tag{B.11}$$

$$= \frac{1}{4\pi} I_I K w^2 \int_{-\infty}^{\infty} e^{-ik_x\epsilon_x} e^{\left(-k_x^2\left(\frac{w^2}{4}+Dt\right)\right)} dk_x \int_{-\infty}^{\infty} e^{-ik_y\epsilon_y} e^{\left(-k_y^2\left(\frac{w^2}{4}+Dt\right)\right)} dk_y \tag{B.12}$$

$$= I_I K \frac{w^2}{w^2 + 4Dt} \exp\left(-\frac{x'^2 + y'^2}{w^2 + 4Dt}\right). \tag{B.13}$$

Therefore, we get for $c(x, y, t)$:

$$c(x, y, t) = I_I \left(1 - K \frac{w^2}{w^2 + 4Dt} \exp\left(-\frac{(x - b_1)^2 + (y - b_2)^2}{w^2 + 4Dt}\right)\right). \tag{B.14}$$

In order to evaluate the intensity inside the whole bleached circle of radius R, we need to integrate Equation B.14 in polar coordinates:

$$I_{2D}(t) = \int_0^R 2\pi r I_I \left(1 - K \frac{w^2}{w^2 + 4Dt} \exp\left(-\frac{r^2}{w^2 + 4Dt}\right)\right) dr \tag{B.15}$$

$$\text{with } \int x e^{-ax^2} dx = -\frac{1}{2a} e^{-ax^2} \tag{B.16}$$

$$= \left[\pi r^2 I_I\right]_0^R - 2\pi I_I K \frac{w^2}{w^2 + 4Dt} \left[-\frac{1}{2}(w^2 + 4Dt) \exp\left(-\frac{r^2}{w^2 + 4Dt}\right)\right]_0^R \tag{B.17}$$

$$= \pi R^2 I_I - \pi I_I K w^2 \left(1 - \exp\left(-\frac{R^2}{w^2 + 4Dt}\right)\right) \tag{B.18}$$

$$= \pi R^2 I_I \left(1 - K \frac{w^2}{R^2} \left[1 - \exp\left(-\frac{R^2}{w^2 + 4Dt}\right)\right]\right), \tag{B.19}$$

which, after redefining I_I and incorporating the term taking into account the immobile fraction, is equal to Equation 2.11.

Appendix C

MATLAB script: 1D FRAP analysis on planar SLBs

```
%%%%%%%%%%%%%%%%%%%%%%%%%%%%%%%%%%%%%%%%%%%%%%%%%%%%%%%%%%%%%%%%%%%%%%%%%%%%%%%%
%                                                                                 %
%       The image should be cropped in a SQUARE around the middle                 %
%                                                                                 %
%%%%%%%%%%%%%%%%%%%%%%%%%%%%%%%%%%%%%%%%%%%%%%%%%%%%%%%%%%%%%%%%%%%%%%%%%%%%%%%%

close all
clear all

%%%%%%%%%%%%%%%%%%%%%%%%%%%%%%%%%%%%%%%%%%%%%%%%%%%%%%%%%%%%%%%%%%%%%%%%%%%%%%%%
%                                   User change                                   %
%%%%%%%%%%%%%%%%%%%%%%%%%%%%%%%%%%%%%%%%%%%%%%%%%%%%%%%%%%%%%%%%%%%%%%%%%%%%%%%%

% file directory
filename = '10_FRAP8_line_1min_laser10_cropped.tif';

% indices of the images that indicate the start and end of the recovery
post_bleach_start = 8;
post_bleach_end = 60;

% indices of the prebleached images (three prebleached images are averaged
% for the normalization)
pre_bleach_nbr1 = 1;
pre_bleach_nbr2 = 2;
pre_bleach_nbr3 = 3;

dx = 0.2166666;    % length of 1 pixel in um
dt = 1;                   % time step between the slides in seconds

% indices of the images that are supposed to be plotted
plot1 = post_bleach_start;
plot2 = post_bleach_start+10;
plot3 = post_bleach_end-3;

% length that the scale bar should have in um
scale = 10;

%%%%%%%%%%%%%%%%%%%%%%%%%%%%%%%%%%%%%%%%%%%%%%%%%%%%%%%%%%%%%%%%%%%%%%%%%%%%%%%%
```

```
%                                                                                %
%%%%%%%%%%%%%%%%%%%%%%%%%%%%%%%%%%%%%%%%%%%%%%%%%%%%%%%%%%%%%%%%%%%%%%%%%%%%%%%

% Make a vector with the times starting at t = 0
t = [0:1:post_bleach_end-1];
t = t.*dt;

% Read the prebleach images and average them
Ipre1 = imread(filename,pre_bleach_nbr1);
Ipre2 = imread(filename,pre_bleach_nbr2);
Ipre3 = imread(filename,pre_bleach_nbr3);

Ipre1 = Ipre1 - 400;    % subtract dark count (400)
Ipre2 = Ipre2 - 400;
Ipre3 = Ipre3 - 400;

Ipre = (Ipre1 + Ipre2 + Ipre3)./3.0;

    % show pre-bleach image
    show1 = figure(1); clf;
    imshow(Ipre,[])
        set(show1,'units','points', 'Position', [10 10 500 500])
    line([size(Ipre,2)-6*scale,size(Ipre,2)-6*scale+scale./dx], ...
         [size(Ipre,1)-25, size(Ipre,1)-25],'LineWidth',4,'Color',[1 1 1])

% distance vector, amount of pixels
x = [0:1:size(Ipre,2)-1];
x = x.*dx;

% Read the first postbleach image to determine the center of the bleached
% region p(3)
I = imread(filename,post_bleach_start);
I = I-400;

    % plot non-normalized image for comparison
    show2 = figure(2); clf;
    imshow(I, [])
        set(show2,'units','points', 'Position', [10 10 500 500])
    line([size(I,2)-6*scale,size(I,2)-6*scale+scale./dx], ...
         [size(I,1)-25, size(I,1)-25], 'LineWidth',4,'Color',[1 1 1])

% normalize first post-bleach image with Ipre
I2 = double(I)./double(Ipre);

% take the line profile
Iline = mean(I2(round(size(I2,1))-150:round(size(I2,1))-50,:),1);
% guess for the parameters of the fit p0
[Imin,nmin] = min(Iline);      % Imin: minimum intensity value,
                               % nmin: index of that in Iline
p0 = [Iline(1),Iline(1)-min(Iline),x(nmin),x(nmin)/5];

% fit of the profile at t = 0 to I = a-b*exp(-(x-c).^2/d^2)
fit1 = fit(x', Iline', 'a-b*exp(-(x-c).^2/d^2)','Lower', [0,0,0,0], ...
     'Upper', [Inf,Inf,Inf,Inf], 'startpoint', p0);

% extract coefficients from fit
p = zeros(4,1);
coeff1 = coeffvalues(fit1);
```

```
    p(1) = coeff1(1);
    p(2) = coeff1(2);
    p(3) = coeff1(3);
    p(4) = coeff1(4);

% fit of the line profile for plotting
Iline_fit=p(1)-p(2)*exp(-(x-p(3)).^2/p(4)^2);

% plot the line profile and the fit
figure(3)
plot(x,Iline,'k.',x,Iline_fit,'r-','LineWidth',2)
xlabel('x [\mum]','FontSize',20)
ylabel('Relative intensity','FontSize',20)
set(gca, 'Fontsize', 20)
axis([0 x(end) 0 Iline(1)+0.15])

 Imin = zeros(size(t));  % allocate space for intensity at the center of
                         % the bleached spot at all time steps
 Iright = zeros(size(t));% allocate space for intensity to the right in the
                         % image, outside bleached area --> to account for
                         % bleaching
 Inorm_all = zeros(size(t));

 for i = 1:post_bleach_end      % extract the minimum and right-border
                                % itensities from all images
  % Read the postbleach image(s) and subtract dark count
  I = imread(filename,i);
  I = I-400;

  I2 = double(I)./double(Ipre); % normalize using Ipre
  Iline = mean(I2(round(size(I2,1)/2)-50:round(size(I2,1)/2)+50,:),1);

  % line across connecting the ends of the profile to account for uneven
  % bleaching
  xnorm = linspace(0,x(end),size(x,2));
  Inorm_hold = (mean(Iline(1:10))-mean(Iline(end-10:end)))/x(end).*(-xnorm) ...
             + mean(Iline(1:10));
  Inorm_all(i) = Inorm_hold(nmin);

  Imin(i) = interp1(x,Iline,p(3));%interpolates the value at the position
                                  %p(3) = center of the bleached region
  Imin(i) = Imin(i)/Inorm_hold(nmin);  % region

            [I_min,n_min] = min(Iline);     % Imin: minimum intensity value,
                                            % nmin: index of that in Iline
            p_hold0 = [Iline(1),Iline(1)-min(Iline),x(n_min),x(n_min)/5];

            % fit of the profile at t = 0 to I = a-b*exp(-(x-c).^2/d^2)
            fit_hold = fit(x', (Iline./Inorm_hold)', 'a-b*exp(-(x-c).^2/d^2)', ...
            'Lower', [0,0,0,0], 'Upper', [Inf,Inf,Inf,Inf], 'startpoint', p_hold0);

            % extract coefficients from fit
            p_h = zeros(4,1);
            coeff_h = coeffvalues(fit_hold);
            p_h(1) = coeff_h(1);
            p_h(2) = coeff_h(2);
            p_h(3) = coeff_h(3);
            p_h(4) = coeff_h(4);
```

```
            % fit of the line profile for plotting
            Iline_fit = p_h(1)-p_h(2)*exp(-(x-p_h(3)).^2/p_h(4)^2);

  figure(100); clf;
  plot(x,Iline./Inorm_hold, 'k.', 'markersize',20)
  hold on
  plot(x,Iline_fit,'r-','LineWidth',2)
  axis([0 x(end) 0 1.15])
  %pause

  if i == plot1
                plot1_fit = Iline_fit;
            elseif i == plot2
                plot2_fit = Iline_fit;
            elseif i == plot3
                plot3_fit = Iline_fit;
            else
                continue
            end
 end

% fit of the post-bleach data to I = a*(1-b*sqrt(w0^2./(w0^2+4*c*t)))
c0 = [p(1),p(2),1];
w0 = p(4);      % "radius" of the bleached region at t = 0

ft = fittype('a*(1-b*sqrt(w0^2./(w0^2+4*c*t))-d)', 'problem', 'w0', ...
    'independent', 't');
fit2 = fit((t(post_bleach_start:end)-t(post_bleach_start))', ...
    Imin(post_bleach_start:end)', ft, 'problem', w0,'Lower', [0,0,0,0], ...
    'Upper', [Inf,Inf,Inf,Inf], 'startpoint', [c0,0.1])

% extract coefficients
c = coeffvalues(fit2);

% make a curve of the fitted values, note that post_bleach_start
% corresponds to t=0 s
t2 = linspace(0,t(end)-t(post_bleach_start),100);
Imin_fit = c(1)*(1-c(2)*sqrt(w0^2./(w0^2+4*c(3)*t2))-c(4));

        % plot the data and the fit
        figure(5); clf;
        plot(t([1:pre_bleach_nbr3,post_bleach_start:end]), ...
             Imin([1:pre_bleach_nbr3,post_bleach_start:end]),'k.', ...
             'Markersize',10)
           hold on
        plot(t2+t(post_bleach_start),Imin_fit,'r-','LineWidth',2)
           xlabel('t [s]','FontSize',20)
           ylabel('Relative intensity','FontSize',20)
           legend('I(center)','Fit')
           axis([0 t(end) 0 1.2])
           set(gca,'FontSize',20)

% extract diffusion constant and mobile+immobile fractions
disp(['D = ',num2str(c(3)),' um^2/s']) % diffusion coefficient

I_e = c(1)*(1-c(4));                  % intensity at end of the recovery
I_0 = c(1)*(1-c(2)-c(4));             % intensity right after bleaching
```

```
I_i = c(1);                              % intensity before bleaching

F_m = (I_e - I_0)/(I_i - I_0);
F_im = 1 - F_m;

      disp(['mobile fraction = ',num2str(F_m*100), ' %'])
      disp(['immobile fraction = ',num2str(F_im*100), ' %'])

    % plot three images and their profiles - read in the images (account
    % for dark count and normalize with Ipre) and determine profiles of
    % 10px centered around the center of the bleached region
    I_show1 = imread(filename,plot1);
    I_show1 = I_show1-400;
    I_show1 = double(I_show1)./double(Ipre);
    prof1 = mean(I_show1(round(size(I2,1)/2)-50:round(size(I2,1)/2)+50, ...
            :),1);

    I_show2 = imread(filename,plot2);
    I_show2 = I_show2-400;
    I_show2 = double(I_show2)./double(Ipre);
    prof2 = mean(I_show2(round(size(I2,1)/2)-50:round(size(I2,1)/2)+50, ...
            :),1);

    I_show3 = imread(filename,plot3);
    I_show3 = I_show3-400;
    I_show3 = double(I_show3)./double(Ipre);
    prof3 = mean(I_show3(round(size(I2,1)/2)-50:round(size(I2,1)/2)+50, ...
            :),1);

       % show the three images with scale bars
       show7 = figure(7); clf;
       imshow(I_show1, []);
            set(show7,'units','points', 'Position', [10 10 500 500])
       line([size(I_show1,2)-6*scale,size(I_show1,2)-6*scale+scale./dx],...
            [size(I2,1)-25, size(I2,1)-25], 'LineWidth',4,'Color',[1 1 1])

       show8 = figure(8); clf;
       imshow(I_show2, []);
            set(show8,'units','points', 'Position', [10 10 500 500])
       line([size(I_show1,2)-6*scale,size(I_show1,2)-6*scale+scale./dx],...
            [size(I2,1)-25, size(I2,1)-25], 'LineWidth',4,'Color',[1 1 1])

       show9 = figure(9); clf;
       imshow(I_show3, []);
            set(show9,'units','points', 'Position', [10 10 500 500])
       line([size(I_show1,2)-6*scale,size(I_show1,2)-6*scale+scale./dx],...
            [size(I2,1)-25, size(I2,1)-25], 'LineWidth',4,'Color',[1 1 1])

        xnorm = linspace(0,x(end),size(x,2));

        Inorm1 = (mean(prof1(1:10))-mean(prof1(end-10:end)))/x(end).* ...
                 (-xnorm) + mean(prof1(1:10));
        Inorm2 = (mean(prof2(1:10))-mean(prof2(end-10:end)))/x(end).* ...
                 (-xnorm) + mean(prof2(1:10));
        Inorm3 = (mean(prof3(1:10))-mean(prof3(end-10:end)))/x(end).* ...
                 (-xnorm) + mean(prof3(1:10));

        % plot the profiles of all three images in one figure
```

```
figure(10); clf;
plot(x, prof1./Inorm1, 'k.', 'markersize',10);
    hold on
plot(x, prof2./Inorm2, 'r.', 'markersize',10);
plot(x, prof3./Inorm3, '.', 'Color',[0 0.3 0.8],'markersize', 10);
% plot(x, Inorm1, x, Inorm2, x, Inorm3)
plot(x, plot1_fit, 'k-', 'Linewidth', 2);
plot(x, plot2_fit, 'r-', 'Linewidth', 2);
plot(x, plot3_fit, '-', 'Color', [0 0.3 0.8], 'Linewidth', 2);

legend(['t = ',num2str(t(plot1)-t(post_bleach_start)),'s'], ...
       ['t = ',num2str(t(plot2)-t(post_bleach_start)),'s'], ...
       ['t = ',num2str(t(plot3)-t(post_bleach_start)),'s'], ...
       'location', 'best')
xlabel('r [\mum]', 'Fontsize',20)
ylabel('Relative Intensity', 'Fontsize',20)
set(gca, 'Fontsize', 20)
axis([0 x(end) 0 prof1(1)+0.15])
```

Appendix D

MATLAB script: 2D FRAP analysis on planar SLBs

```
%%%%%%%%%%%%%%%%%%%%%%%%%%%%%%%%%%%%%%%%%%%%%%%%%%%%%%%%%%%%%%%%%%%%%%%%%%%%%%%%
%                                                                                %
%    The image needs to be cropped in a SQUARE around the bleached spot          %
%                                                                                %
%%%%%%%%%%%%%%%%%%%%%%%%%%%%%%%%%%%%%%%%%%%%%%%%%%%%%%%%%%%%%%%%%%%%%%%%%%%%%%%%

close all
clear all

%%%%%%%%%%%%%%%%%%%%%%%%%%%%%%%%%%%%%%%%%%%%%%%%%%%%%%%%%%%%%%%%%%%%%%%%%%%%%%%%
%                                   User change                                  %
%%%%%%%%%%%%%%%%%%%%%%%%%%%%%%%%%%%%%%%%%%%%%%%%%%%%%%%%%%%%%%%%%%%%%%%%%%%%%%%%

% file directory
filename = '07_FRAP5_1min_laser10_cropped.tif';
% indices of the prebleached images (three prebleached images are averaged
% for the normalization)
pre_bleach_nbr1 = 1;
pre_bleach_nbr2 = 2;
pre_bleach_nbr3 = 3;

% indices of the images that indicate the start and end of the recovery
post_bleach_start = 7;
post_bleach_end = 60;

dt = 1;                % time step in seconds between slides
dx = 0.21666;          % size in um of one pixel

% indices of the images that are supposed to be plotted
plot1 = post_bleach_start;
plot2 = post_bleach_start+10;
plot3 = post_bleach_end-3;

% length that the scale bar should have in um
scale = 10;

%%%%%%%%%%%%%%%%%%%%%%%%%%%%%%%%%%%%%%%%%%%%%%%%%%%%%%%%%%%%%%%%%%%%%%%%%%%%%%%%
%                                                                                %
```

```
%%%%%%%%%%%%%%%%%%%%%%%%%%%%%%%%%%%%%%%%%%%%%%%%%%%%%%%%%%%%%%%%%%%%%%%%%%%%%%%%

% Make a vector with the times starting at t = 0
t = [0:1:post_bleach_end-1];
t = t.*dt;

% Read the prebleach images and average them to Ipre
Ipre1 = imread(filename, pre_bleach_nbr1);
Ipre2 = imread(filename, pre_bleach_nbr2);
Ipre3 = imread(filename, pre_bleach_nbr3);

Ipre1 = Ipre1 - 400;    % subtract dark count (400)
Ipre2 = Ipre2 - 400;
Ipre3 = Ipre3 - 400;

Ipre = (Ipre1+Ipre2+Ipre3)./3.0;

    % show pre-bleach image
    show4 = figure(4); clf; imshow(Ipre,[])
        set(show4,'units','points', 'Position', [10 10 500 500])
    line([size(Ipre,2)-6*scale,size(Ipre,2)-6*scale+scale./dx],...
         [size(Ipre,1)-25, size(Ipre,1)-25], 'LineWidth',4,'Color',[1 1 1])

% distance vectors in x- and y-direction
x = [0:1:size(Ipre,2)-1];
x = x.*dx;

y = [0:1:size(Ipre,1)-1];
y = y.*dx;

% Read the first postbleach image
I = imread(filename,post_bleach_start);
I = I-400;
    % plot non-normalized image for comparison
    show5 = figure(5); clf;
    imshow(I, [])
        set(show5,'units','points', 'Position', [10 10 500 500])
    line([size(I,2)-6*scale,size(I,2)-6*scale+scale./dx],...
          [size(I,1)-25, size(I,1)-25], 'LineWidth',4,'Color',[1 1 1])

    % normalize with Ipre
I2 = double(I)./double(Ipre);

    % take the line profile along x and y
profile_x = mean(I2(round(size(I2,1)/2-5):round(size(I2,1)/2+5),:),1);
profile_y = mean(I2(:,round(size(I2,2)/2-5):round(size(I2,2)/2+5)),2);
     % plot of the chosen profile
     %figure(1); clf; plot(x, profile_y, 'k.')

    % initial guess for the coefficients in the profile fit
[Imin_x ,xmin_x] = min(profile_x); % returns x and y of the minimum in the
                                   % x-profile
px0 = [profile_x(1), profile_x(1)-min(profile_x), x(xmin_x), x(xmin_x)/5];

[Imin_y ,xmin_y] = min(profile_y); % returns x and y of the minimum in the
                                   % y-profile
py0 = [profile_y(1), profile_y(1)-min(profile_y), y(xmin_y), y(xmin_y)/5];
```

```
% fit intensity profile to formula (1) from Johansson et al. (2014)
fit1x = fit(x', profile_x', 'I_0*(1-K*exp(-(x-b)^2/w^2))',...
       'Lower', [0,0,0,0],'Upper',[Inf,Inf,Inf,Inf], 'startpoint', ...
       px0);
fit1y = fit(y', profile_y, 'I_0*(1-K*exp(-(x-b)^2/w^2))',...
       'Lower', [0,0,0,0],'Upper',[Inf,Inf,Inf,Inf], 'startpoint', ...
       py0);

    % plot fit in x-direction
    show2 = figure(2); clf;
        %set(show2,'units','points', 'Position', [10 10 500 500])
        handle_fit1 = plot(fit1x, 'r-');
        set(handle_fit1, 'linewidth',2)
    hold on
    plot(x, profile_x, 'k.', 'markersize',20)
        legend('hide')
        xlabel('r [\mum]','fontsize',20)
        ylabel('Intensity','fontsize',20)
        set(gca,'fontsize',20)
        axis([0 x(end) 0 profile_x(1)+0.15])

    % extract coefficients for subsequent fit
    coeff1 = coeffvalues(fit1x);
    w = coeff1(4);
    R = w/sqrt(2); % radius of bleached region
    K = coeff1(2);

% fit for circular diffusion, formula (2) from Johansson et al. (2014)
    % create a fittype that lets me read in w, K and R as determined
    % previously
ft = fittype(...
'a*(1-w^2*K/R^2*(1-exp(-R^2/(w^2+4*d*x)))-K_im*w^2/R^2*(1-exp(-R^2/w^2)))', ...
'problem', {'w','R','K'});

    % find minima of the functions in x and y --> to find center of
    % bleached spot
    [min_fit1x_x, min_fit1x_y] = fminbnd(fit1x, xmin_x*dx-30,xmin_x*dx+30);
    [min_fit1y_x, min_fit1y_y] = fminbnd(fit1y, xmin_y*dx-30,xmin_y*dx+30);

    % choose a circular ROI with radius R positioned in the center of the
    % bleached spot
    t_ROI = 0:pi/30:2*pi;

    x_ROI = R/dx*cos(t_ROI) + min_fit1x_x/dx;
    y_ROI = R/dx*sin(t_ROI) + min_fit1y_x/dx;

    ROI = roipoly(I2, x_ROI, y_ROI);
        % plot circular ROI
        figure(3); clf; imshow(ROI);

           % choose a second and third ROI outside the bleached spot to
           % account for bleaching (2 rectangles spanning the whole length
           % of the image on the top and the bottom of the image)

           x_bleach = [10, 10, size(I2,2)-10, size(I2,2)-10];
           y_bleach = [10, size(I2,1)/4, size(I2,1)/4,10];
           ROI_bleach = roipoly(I2, x_bleach, y_bleach);
```

```
            y_bleach2 = [size(I2,1)-60, size(I2,1)-10, size(I2,1)-10, ...
                size(I2,1)-60];
            ROI_bleach2 = roipoly(I2, x_bleach, y_bleach2);

                % plot "bleaching" ROI
                figure(3); clf; imshow(ROI_bleach2);

    % allocate space for intensity inside the circular ROI
    intensity = zeros(post_bleach_end-post_bleach_start+1,1);
    I_bleach = zeros(1:post_bleach_end,1);

    % get the mean intensity in the circular ROI for all images
    for i = 1:post_bleach_end

        Im = imread(filename,i);
        Im = Im - 400;                      % subtract dark count
        Im2 = double(Im)./double(Ipre);     % normalize with Ipre
        Ibleach1 = mean(Im2(ROI_bleach));
        Ibleach2 = mean(Im2(ROI_bleach2));
        Ibleach(i) = (Ibleach1+Ibleach2)/2.0;% average the intensity in the
                                             % two bleaching ROIs
        Im3 = double(Im2)./double(Ibleach(i)); % normalize with bleached I
        intensity(i) = mean(Im3(ROI));

    end

fit2 = fit((t(post_bleach_start:end)-t(post_bleach_start))', ...
    intensity(post_bleach_start:post_bleach_end), ft, 'problem',{w,R,K},...
    'Lower', [0,0,0],'Upper',[Inf,Inf,Inf], 'startpoint', [0.1,1,3]);

    % extract coefficients from fit for the plot
    coeff3 = coeffvalues(fit2);
        K_im = coeff3(1);
        a = coeff3(2);
    t2 = linspace(0,t(end)-t(post_bleach_start),100);
    I_final= coeff3(2)*(1-w^2*K./R^2*(1-exp(-R^2./(w^2+4*coeff3(3)...
             *t2)))-coeff3(1)*w^2/R^2*(1-exp(-R^2/w^2)));

    % plot recovery data
    figure(6); clf;
    plot(t2+t(post_bleach_start), I_final, 'r-','linewidth',2)
    hold on
    plot(t([1:pre_bleach_nbr3,post_bleach_start:end])', ...
        intensity([1:pre_bleach_nbr3,post_bleach_start:end]), ...
        'k.', 'markersize',20)
    xlabel('time [s]', 'fontsize',20)
    ylabel('Relative Intensity', 'fontsize',20)
    set(gca, 'fontsize', 20)

% extract diffusion coefficient from fit
disp(['Diffusion constant: D = ',num2str(coeff3(3)),' um^2/s'])

% extract mobile and immobile fraction from fit
    K1_prime = w^2*K./R^2*(1-exp(-R^2./w^2));
    K2_prime = w^2*K_im./R^2*(1-exp(-R^2./w^2));
I_e = a*(1-K2_prime);               % intensity at end of the recovery
I_0 = a*(1-K1_prime-K2_prime);      % intensity right after bleaching
```

```
I_i = a;                              % intensity before bleaching

F_m = (I_e - I_0)/(I_i - I_0);
F_im = 1 - F_m;

disp(['mobile fraction: F_m = ',num2str(F_m*100), ' %'])
disp(['immobile fraction: F_im = ',num2str(F_im*100), ' %'])

    % plot three images and their profiles - read in the images (account
    % for dark count and normalize with Ipre) and determine profiles of
    % 10px centered around the center of the bleached region
    I_show1 = imread(filename,plot1);
    I_show1 = I_show1-400;
    I_show1 = double(I_show1)./double(Ipre);
    prof1 = mean(I_show1(round(xmin_y-5):round(xmin_y+5),:),1);

    I_show2 = imread(filename,plot2);
    I_show2 = I_show2-400;
    I_show2 = double(I_show2)./double(Ipre);
    prof2 = mean(I_show2(round(xmin_y-5):round(xmin_y+5),:),1);

    I_show3 = imread(filename,plot3);
    I_show3 = I_show3-400;
    I_show3 = double(I_show3)./double(Ipre);
    prof3 = mean(I_show3(round(xmin_y-5):round(xmin_y+5),:),1);

        % Inorm{i} is a line connecting the ends of the respective profile
        % of number {i} in order to account for the uneven bleaching across
        % the slide
        xnorm = linspace(0,x(end),size(x,2));

        Inorm1 = (mean(prof1(1:10))-mean(prof1(end-10:end)))/x(end).* ...
                 (-xnorm) + mean(prof1(1:10));
        Inorm2 = (mean(prof2(1:10))-mean(prof2(end-10:end)))/x(end).* ...
                 (-xnorm) + mean(prof2(1:10));
        Inorm3 = (mean(prof3(1:10))-mean(prof3(end-10:end)))/x(end).* ...
                 (-xnorm) + mean(prof3(1:10));

        plot1_fit = fit(x', (prof1./Inorm1)', 'I_0*(1-K*exp(-(x-b)^2/w^2))',...
       'Lower', [0,0,0,0],'Upper',[Inf,Inf,Inf,Inf], 'startpoint', ...
        px0);
        plot2_fit = fit(x', (prof2./Inorm2)', 'I_0*(1-K*exp(-(x-b)^2/w^2))',...
       'Lower', [0,0,0,0],'Upper',[Inf,Inf,Inf,Inf], 'startpoint', ...
        px0);
        plot3_fit = fit(x', (prof3./Inorm3)', 'I_0*(1-K*exp(-(x-b)^2/w^2))',...
       'Lower', [0,0,0,0],'Upper',[Inf,Inf,Inf,Inf], 'startpoint', ...
        px0);

       % show the three images with scale bars
       show1 = figure(7); clf;
       imshow(I_show1./Ibleach(plot1), []);
            set(show1,'units','points', 'Position', [10 10 500 500])
       line([size(I_show1,2)-6*scale,size(I_show1,2)-6*scale+scale./dx],...
            [size(I2,1)-25, size(I2,1)-25], 'LineWidth',4,'Color',[1 1 1]);

       show2 = figure(8); clf;
       imshow(I_show2./Ibleach(plot2), []);
            set(show2,'units','points', 'Position', [10 10 500 500])
```

```
line([size(I_show1,2)-6*scale,size(I_show1,2)-6*scale+scale./dx],...
     [size(I2,1)-25, size(I2,1)-25], 'LineWidth',4,'Color',[1 1 1]);

show3 = figure(9); clf;
hhh = imshow(I_show3./Ibleach(plot3), []);
     set(show3,'units','points', 'Position', [1 1 500 500])
line([size(I_show1,2)-6*scale,size(I_show1,2)-6*scale+scale./dx],...
     [size(I2,1)-25, size(I2,1)-25], 'LineWidth',4,'Color',[1 1 1]);

 % plot the profiles of all three images in one figure
 figure(10); clf;
 plot(x, prof1./Inorm1, 'k.', 'markersize',10);
     hold on
 plot(x, prof2./Inorm2, 'r.', 'markersize',10);
 plot(x, prof3./Inorm3, '.', 'Color', [0 0.3 0.8],'markersize',10);

 handle_fit1 = plot(plot1_fit, 'k-');
 set(handle_fit1, 'linewidth',2)
 handle_fit2 = plot(plot2_fit, 'r-');
 set(handle_fit2, 'linewidth',2)
 handle_fit3 = plot(plot3_fit, '-');
 set(handle_fit3, 'linewidth',2,'Color', [0 0.3 0.8])

 legend(['t = ',num2str(t(plot1)-t(post_bleach_start)),'s'], ...
        ['t = ',num2str(t(plot2)-t(post_bleach_start)),'s'], ...
        ['t = ',num2str(t(plot3)-t(post_bleach_start)),'s'], ...
        'location', 'best')
 xlabel('r [\mum]', 'Fontsize',20)
 ylabel('Relative Intensity', 'Fontsize',20)
 set(gca, 'Fontsize', 20)
 axis([0 x(end) 0 prof1(1)+0.15])
```

Appendix E

MATLAB script: 1D FRAP analysis on pipette SLBs

```
close all
clear all

%%%%%%%%%%%%%%%%%%%%%%%%%%%%%%%%%%%%%%%%%%%%%%%%%%%%%%%%%%%%%%%%%%%%%%%%%%%%%%%%
%                                   User change                                   %
%%%%%%%%%%%%%%%%%%%%%%%%%%%%%%%%%%%%%%%%%%%%%%%%%%%%%%%%%%%%%%%%%%%%%%%%%%%%%%%%

% file directory of the FRAP
filename = '08_FRAP_laser10_20min_cropped.tif';

% file directory of the pre-bleach image
pre_bleach = '07_prebleach_filter1_laser10_cropped.tif';

% indices of the images that indicate the start and end of the recovery
post_bleach_start = 1;
post_bleach_end = 239;

dt = 5;             % time step in seconds between slides
dx = 0.65;          % size in um of one pixel

% indices of the images that are supposed to be plotted
plot1 = post_bleach_start;
plot2 = post_bleach_start+100;
plot3 = post_bleach_end-50;

% length that the scale bar should have in um
scale = 10;

%%%%%%%%%%%%%%%%%%%%%%%%%%%%%%%%%%%%%%%%%%%%%%%%%%%%%%%%%%%%%%%%%%%%%%%%%%%%%%%%
%                                                                                 %
%%%%%%%%%%%%%%%%%%%%%%%%%%%%%%%%%%%%%%%%%%%%%%%%%%%%%%%%%%%%%%%%%%%%%%%%%%%%%%%%

% Make a vector with the times starting at t = 0
t = [0:1:post_bleach_end-1];
t = t.*dt;

% Read the prebleach image
Ipre = imread(pre_bleach);
```

```
% subtract dark count
Ipre = Ipre - 400;

    % show pre-bleach image
    show1 = figure(1); clf; imshow(Ipre,[])
        set(show1,'units','points', 'Position', [0 0 400 300])
    line([size(Ipre,2)-3*scale,size(Ipre,2)-3*scale+scale./dx],...
         [size(Ipre,1)-10, size(Ipre,1)-10], 'LineWidth',4,'Color',[1 1 1])

% distance vector, amount of pixels
x = [0:1:size(Ipre,2)-1];
x = x.*dx;

% Read the first postbleach image and subtract dark count
I = imread(filename,post_bleach_start);
I = I-400;

    % plot non-normalized image for comparison
    show2 = figure(2); clf;
    imshow(I, [])
        set(show2,'units','points', 'Position', [0 0 400 300])
    line([size(I,2)-3*scale,size(I,2)-3*scale+scale./dx],...
         [size(I,1)-10, size(I,1)-10], 'LineWidth',4,'Color',[1 1 1])

% normalize the image with Ipre
I2 = double(I)./double(Ipre);

% choose profile Iline
Iline = mean(I2(round(size(I2,1)/2)-10:round(size(I2,1)/2)+10,:),1);

xnorm = linspace(0,x(end),size(x,2));
Inorm = (mean(Iline(1:10))-mean(Iline(end-10:end)))/x(end).*(-xnorm) ...
            + mean(Iline(1:10));

% guess for the parameters of the fit p0
[Imin,nmin] = min(Iline);      % Imin: minimum intensity value,
                               % nmin: index of that in Iline
p0 = [Iline(1),Iline(1)-min(Iline),x(nmin),x(nmin)/5];

% fit of the profile at t = 0 to I = a-b*exp(-(x-c).^2/d^2)
fit1 = fit(x', (Iline./Inorm)', 'a-b*exp(-(x-c).^2/d^2)', 'Lower', ...
    [0,0,0,0], 'Upper', [Inf,Inf,Inf,Inf], 'startpoint', p0);

% extract coefficients from fit
p = zeros(4,1);
coeff1 = coeffvalues(fit1);
    p(1) = coeff1(1);
    p(2) = coeff1(2);
    p(3) = coeff1(3);
    p(4) = coeff1(4);

% fit of the line profile for plotting
Iline_fit=p(1)-p(2)*exp(-(x-p(3)).^2/p(4)^2);

% plot the line profile and the fit
figure(3)
plot(x,Iline./Inorm,'k.',x,Iline_fit,'r-','LineWidth',2, 'Markersize',10)
```

```
xlabel('x [\mum]','FontSize',20)
ylabel('Relative intensity','FontSize',20)
set(gca, 'Fontsize', 20)
axis([0 x(end) 0 Iline_fit(1)+0.15])

 Imin = zeros(size(t));  % allocate space for intensity at the center of
                         % the bleached spot at all time steps
 Inorm_all = zeros(size(t));

 for i = 1:post_bleach_end      % extract the minimum and right-border
                                % itensities from all images
  % Read the postbleach image(s) and subtract dark count
  I = imread(filename,i);
  I = I-400;

  I2 = double(I)./double(Ipre); % normalize using Ipre
  Iline = mean(I2(round(size(I2,1)/2)-10:round(size(I2,1)/2)+10,:),1);

  % line across connecting the ends of the profile to account for uneven
  % bleaching
  xnorm = linspace(0,x(end),size(x,2));
  Inorm_hold = (mean(Iline(1:10))-mean(Iline(end-10:end)))/x(end).*(-xnorm) ...
              + mean(Iline(1:10));
  Inorm_all(i) = Inorm_hold(nmin);

  Imin(i) = interp1(x,Iline,p(3));% interpolates the value at the position
                                  % p(3) = center of the bleached region
                                  % with the intensity outside the bleached
  Imin(i) = Imin(i)/Inorm_hold(nmin);

            [I_min,nmin] = min(Iline);     % Imin: minimum intensity value,
                                           % nmin: index of that in Iline
            p0 = [Iline(1),Iline(1)-min(Iline),x(nmin),x(nmin)/5];

            % fit of the profile at t = 0 to I = a-b*exp(-(x-c).^2/d^2)
            fit1 = fit(x', (Iline./Inorm_hold)', 'a-b*exp(-(x-c).^2/d^2)', ...
                'Lower', [0,0,0,0], 'Upper', [Inf,Inf,Inf,Inf], 'startpoint', p0);

            % extract coefficients from fit
            p = zeros(4,1);
            coeff1 = coeffvalues(fit1);
            p(1) = coeff1(1);
            p(2) = coeff1(2);
            p(3) = coeff1(3);
            p(4) = coeff1(4);

            % fit of the line profile for plotting
            Iline_fit=p(1)-p(2)*exp(-(x-p(3)).^2/p(4)^2);

  figure(100); clf;
  plot(x,Iline./Inorm_hold, 'k.', 'markersize', 10)
  hold on
  plot(x,Iline_fit,'r-','LineWidth',2)
  axis([0 x(end) 0 1.15])

  %pause
  if i == plot1
               plot1_fit = Iline_fit;
```

```
            elseif i == plot2
                plot2_fit = Iline_fit;
            elseif i == plot3
                plot3_fit = Iline_fit;
            else
                continue
            end
 end

% fit of the post-bleach data to I = a*(1-b*sqrt(w0^2./(w0^2+4*c*t)))
c0 = [p(1),p(2),1];
w0 = p(4);      % "radius" of the bleached region at t = 0

ft = fittype('a*(1-b*sqrt(w0^2./(w0^2+4*c*t))-d)', 'problem', 'w0', ...
    'independent', 't');
fit2 = fit(t', Imin', ft, 'problem', w0,'Lower', [0,0,0,0], ...
    'Upper', [Inf,Inf,Inf,Inf], 'startpoint', [c0,0.1])

% extract coefficients
c = coeffvalues(fit2);

% make a curve of the fitted values, note that post_bleach_start
% corresponds to t=0 s
t2 = 1;
Imin_fit = c(1)*(1-c(2)*sqrt(w0^2./(w0^2+4*c(3)*t))-c(4));

        % plot the data and the fit
        show4 = figure(4); clf;
        plot(t2-1, 1, 'k.', t+t2, Imin, 'k.', 'Markersize',10)
           hold on
        plot(t+t2,Imin_fit,'r-','LineWidth',2)
           xlabel('t [s]','FontSize',20)
           ylabel('Relative intensity','FontSize',20)
           axis([0 t(end) 0 1.2])
           set(gca,'FontSize',20)

% extract diffusion constant and mobile+immobile fractions
disp(['D = ',num2str(c(3)),' um^2/s']) % diffusion coefficient

I_e = c(1)*(1-c(4));                   % intensity at end of the recovery
I_0 = c(1)*(1-c(2)-c(4));              % intensity right after bleaching
I_i = c(1);                            % intensity before bleaching

F_m = (I_e - I_0)/(I_i - I_0);
F_im = 1 - F_m;

    disp(['mobile fraction = ',num2str(F_m*100), ' %'])
    disp(['immobile fraction = ',num2str(F_im*100), ' %'])

    % plot three images and their profiles - read in the images (account
    % for dark count and normalize with Ipre) and determine profiles of
    % 10px centered around the center of the bleached region
    I_show1 = imread(filename,plot1);
    I_show1 = I_show1-400;

    I_show2 = imread(filename,plot2);
    I_show2 = I_show2-400;
```

```
I_show3 = imread(filename,plot3);
I_show3 = I_show3-400;

   % show the three images with scale bars
   show7 = figure(7); clf;
   imshow(I_show1, []);
      set(show7,'units','points', 'Position', [0 0 400 300])
   line([size(I_show1,2)-3*scale,size(I_show1,2)-3*scale+scale./dx],...
        [size(I2,1)-10, size(I2,1)-10], 'LineWidth',4,'Color',[1 1 1])

   show8 = figure(8); clf;
   imshow(I_show2, []);
      set(show8,'units','points', 'Position', [0 0 400 300])
   line([size(I_show1,2)-3*scale,size(I_show1,2)-3*scale+scale./dx],...
        [size(I2,1)-10, size(I2,1)-10], 'LineWidth',4,'Color',[1 1 1])

   show9 = figure(9); clf;
   imshow(I_show3, []);
        set(show9,'units','points', 'Position', [0 0 400 300])
   line([size(I_show1,2)-3*scale,size(I_show1,2)-3*scale+scale./dx],...
        [size(I2,1)-10, size(I2,1)-10], 'LineWidth',4,'Color',[1 1 1])

I_show1 = double(I_show1)./double(Ipre);
I_show2 = double(I_show2)./double(Ipre);
I_show3 = double(I_show3)./double(Ipre);

prof1 = mean(I_show1(round(size(I2,1)/2)-10:round(size(I2,1)/2)+10, ...
        :),1);
prof2 = mean(I_show2(round(size(I2,1)/2)-10:round(size(I2,1)/2)+10, ...
        :),1);
prof3 = mean(I_show3(round(size(I2,1)/2)-10:round(size(I2,1)/2)+10, ...
        :),1);

   xnorm = linspace(0,x(end),size(x,2));

   Inorm1 = (mean(prof1(1:10))-mean(prof1(end-10:end)))/x(end).* ...
             (-xnorm) + mean(prof1(1:10));
   Inorm2 = (mean(prof2(1:10))-mean(prof2(end-10:end)))/x(end).* ...
             (-xnorm) + mean(prof2(1:10));
   Inorm3 = (mean(prof3(1:10))-mean(prof3(end-10:end)))/x(end).* ...
             (-xnorm) + mean(prof3(1:10));

   % plot the profiles of all three images in one figure
   figure(10); clf;
   plot(x, prof1./Inorm1, 'k.', 'markersize',10);
      hold on
   plot(x, prof2./Inorm2, 'r.', 'markersize',10);
   plot(x, prof3./Inorm3, '.', 'Color', [0 0.3 0.8],'markersize', 10);

   plot(x, plot1_fit, 'k-', 'Linewidth', 2);
   plot(x, plot2_fit, 'r-', 'Linewidth', 2);
   plot(x, plot3_fit, '-', 'Color', [0 0.3 0.8], 'Linewidth', 2);

   legend(['t = ',num2str(t(plot1)-t(post_bleach_start)),'s'], ...
          ['t = ',num2str(t(plot2)-t(post_bleach_start)),'s'], ...
          ['t = ',num2str(t(plot3)-t(post_bleach_start)),'s'], ...
          'location', 'best')
   xlabel('r [\mum]', 'Fontsize',20)
```

```
ylabel('Relative Intensity', 'Fontsize',20)
set(gca, 'Fontsize', 20)
axis([0 x(end) 0 1+0.15])
```